

SUPPORTING INFORMATION

Exploring the electrochromic properties of poly(thieno[3,2-*b*]thiophene)s decorated with electron-deficient side groups

Shan Shao,^a Jingjing Shi,^a Imran Murtaza,^{b,c} Panpan Xu,^a Yaowu He,^a Sanjay Ghosh,^d
Xiaosi Zhu,^a Igor. F. Perepichka*^d and Hong Meng*^{a,b}

^a*School of Advanced Materials, Peking University Shenzhen Graduate School, Shenzhen 518055, China. Tel: (86)-18565807998, E-mail: menghong@pkusz.edu.cn*

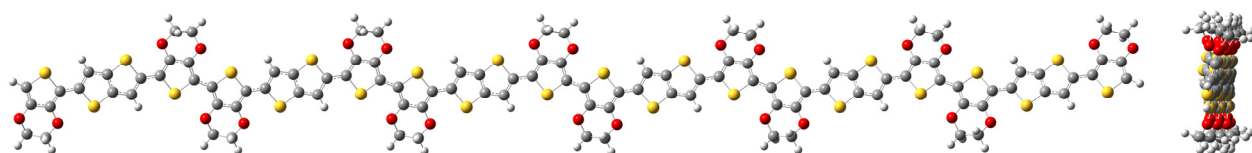
^b*Key Laboratory of Flexible Electronics (KLOFE) & Institute of Advanced Materials (IAM), Jiangsu National Synergetic Innovation Center for Advanced Materials (SICAM), Nanjing Tech University (Nanjing Tech), 30 South Puzhu Road, Nanjing 211816, China*

^c*Department of Physics, International Islamic University, Islamabad 44000, Pakistan*

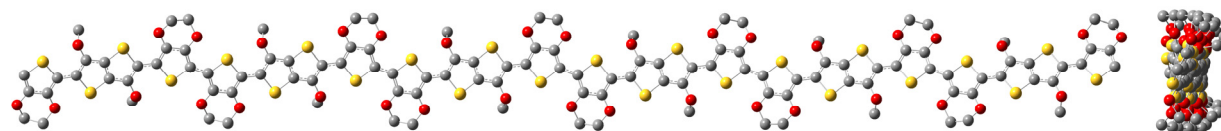
^d*School of Chemistry, Bangor University, Deiniol Road, Bangor LL57 2UW, United Kingdom. E-mail: i.perepichka@bangor.ac.uk*

B3LYP/6-31G(d) calculations for hexamers (R-ETTE)₆ and (EDOT-HTTH)₆

Details of computational procedures are given in the Experimental part of the paper. In the most cases, the geometries were fully optimized with no constrains and all atoms were free to optimize. However, in some cases, calculations of the oligomers from their planar conformations (with alternated signs of the dihedral angles in the EDOT–TT–EDOT fragment) led to change of the signs of the dihedrals during an optimization process to adopt more stable helix conformations (for the whole molecule or for the part of it). In these cases, we pre-optimized the planar geometry to the intermediate state before it started to change its conformation to the helix and restarted calculations with frozen TT-EDOT dihedrals. After optimization to the minimum of energy, the dihedrals were slightly changed (increased or decreased) and the re-optimization was performed several times to find the geometry of the lowest energy with the frozen TT–EDOT dihedrals. For molecules with small dihedrals (as in the cases of (EDOT-HTTH)₆ and (MeTh-ETTE)₆), this required most of the TT–EDOT dihedrals in the middle part of the molecule to be frozen. For molecules with larger dihedrals (as in (CNPh-ETTE)₆), only two dihedrals between the end TT moieties and the neighboring inner EDOT moieties were frozen.

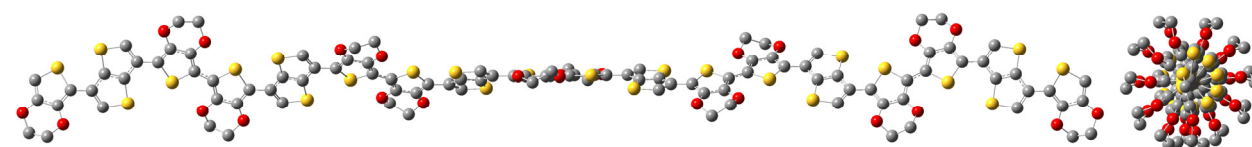


(a) **(H-ETTE)₆**: $E_{\text{total}} = -15514.3469487$ Hartree;
 $\text{S}\cdots\text{O}$ distances are $\sim 2.94\text{--}2.96$ Å (EDOT–EDOT and TT–EDOT); dihedral angles TT–EDOT are $\sim 1.2\text{--}3^\circ$.

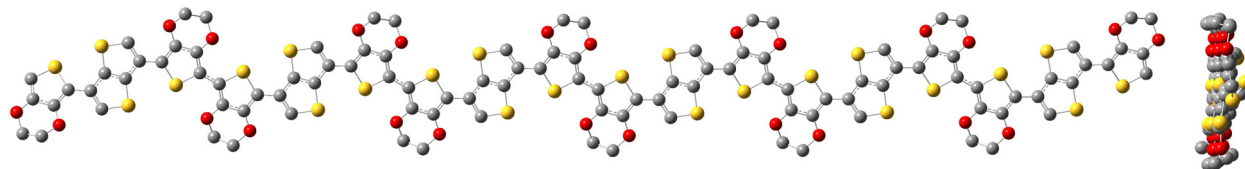


(b) **(MeO-ETTE)₆**: $E_{\text{total}} = -16888.5374032$ Hartree;
 $\text{S}\cdots\text{O}$ distances are ~ 2.94 Å (EDOT–EDOT), $\sim 2.91\text{--}2.93$ Å (EDOT–TT); $\sim 2.89\text{--}2.92$ Å (MeO–EDOT);
dihedral angles TT–EDOT are $\sim 2.9\text{--}5.1^\circ$. Hydrogen atoms are omitted for clarity.

Fig. S1 B3LYP/6-31G(d) optimized geometries of hexamers (a) **(H-ETTE)₆** and (b) **(MeO-ETTE)₆**. Two views are shown, i.e. perpendicular to the main chain (left) and along the main chain (right)



(EDOT-HTTH)₆ / helix, $E_{\text{total}} = -15514.3102867$ Hartree

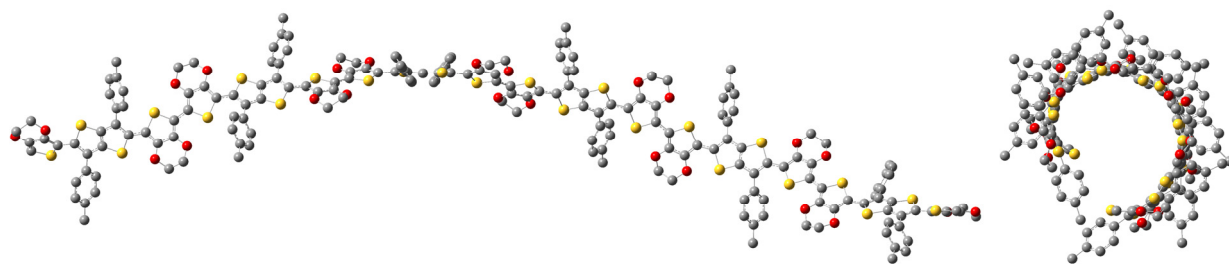


(EDOT-HTTH)₆ / planar, $E_{\text{total}} = -15514.30837$ Hartree*

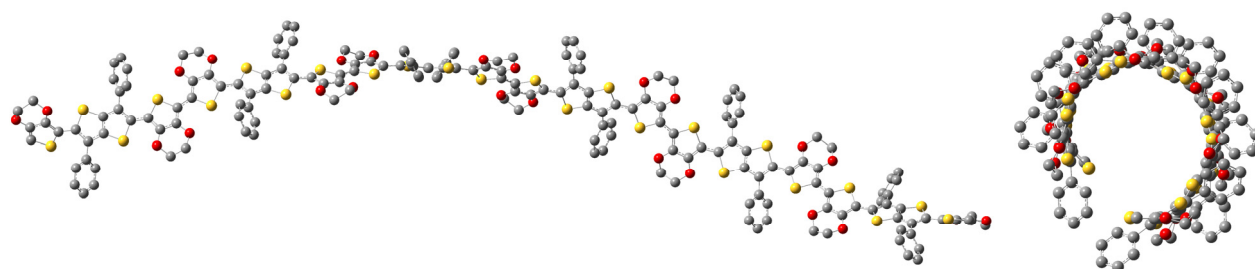
$$\Delta E (\text{helix-planar}) = -5.03 \text{ kJ/mol}$$

Fig. S2 B3LYP/6-31G(d) optimized geometries of helix and planar conformations of the hexamer **(EDOT-HTTH)₆**. Left pictures are the views perpendicular to the main chain and right pictures are the views along the main chain. Hydrogen atoms are omitted for clarity.

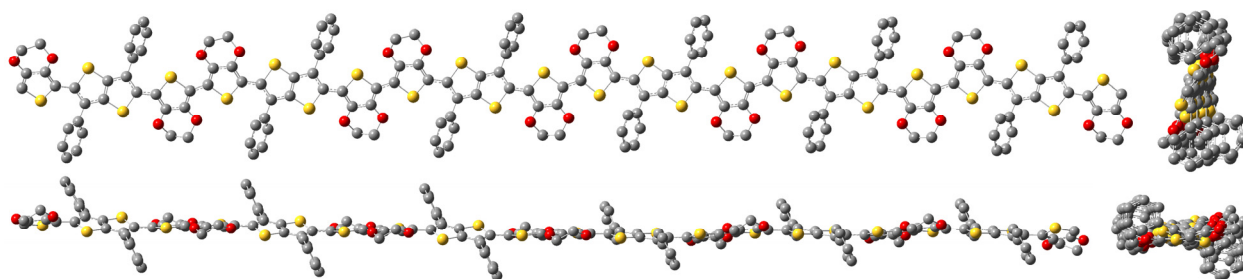
* *Dihedrals at the EDOT–TT–EDOT along the backbone were frozen at $+9^\circ/-9^\circ$ (except at the end monomer units, where dihedrals were free to optimize).*



(MePh-ETTE)₆ / helix, $E_{\text{total}} = -18758.7842414$ Hartree



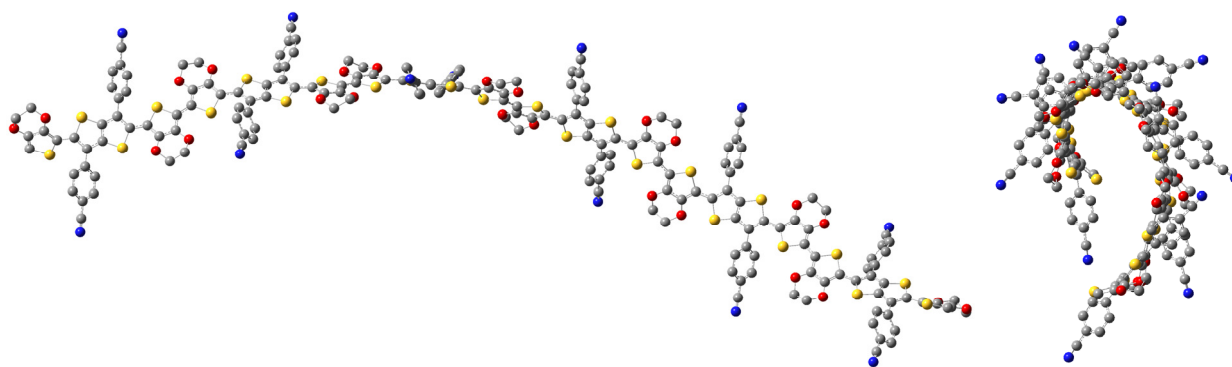
(Ph-ETTE)₆ / helix, $E_{\text{total}} = -18286.9670284$ Hartree



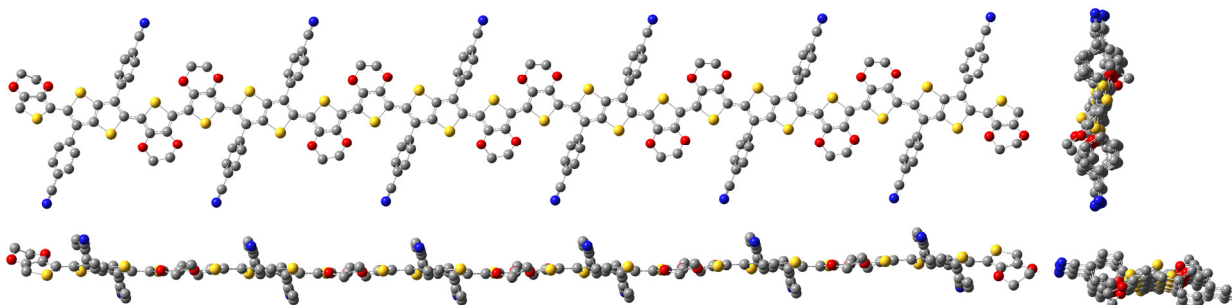
(Ph-ETTE)₆ / planar, $E_{\text{total}} = -18286.9610271$ Hartree

ΔE (helix–planar) = -15.76 kJ/mol

Fig. S3 B3LYP/6-31G(d) optimized geometries of hexamers **(MePh-HTTH)₆** (helix conformation) and **(Ph-HTTH)₆** (both helix and planar conformation). Left pictures are the views perpendicular to the main chain and right pictures are the views along the main chain. Hydrogen atoms are omitted for clarity.



(CNPh-ETTE)₆ / helix, $E_{\text{total}} = -19393.9004055$ Hartree

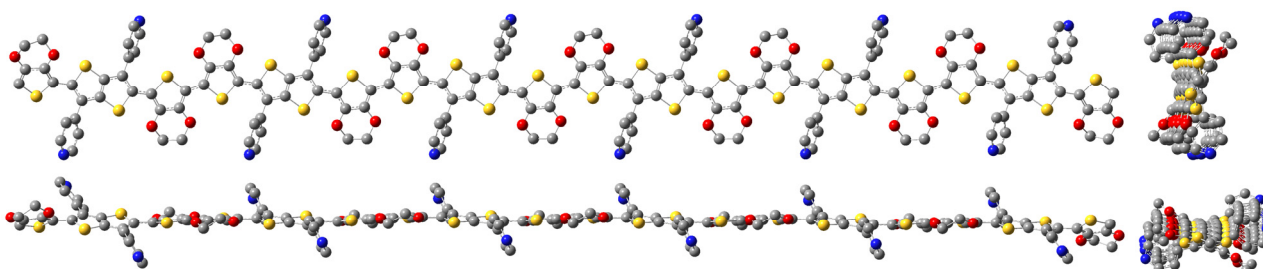


(CNPh-ETTE)₆ / planar, $E_{\text{total}} = -19393.8945301$ Hartree (freeze)*

ΔE (helix–planar) = **-15.43 kJ/mol**



(Py-ETTE)₆ / helix, $E_{\text{total}} = -18479.4111434$ Hartree

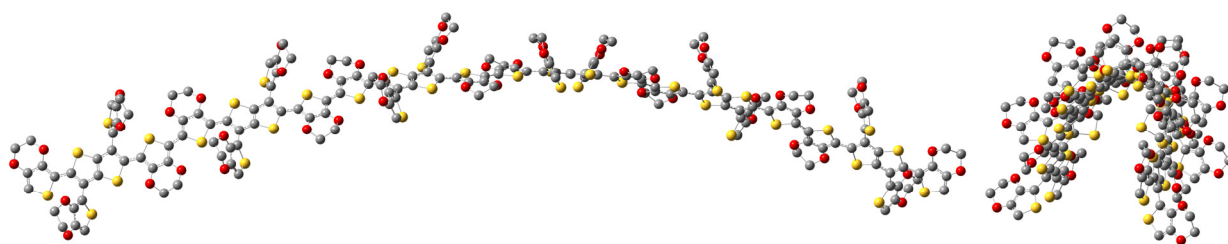


(Py-ETTE)₆ / planar, $E_{\text{total}} = -18479.4047967$ Hartree

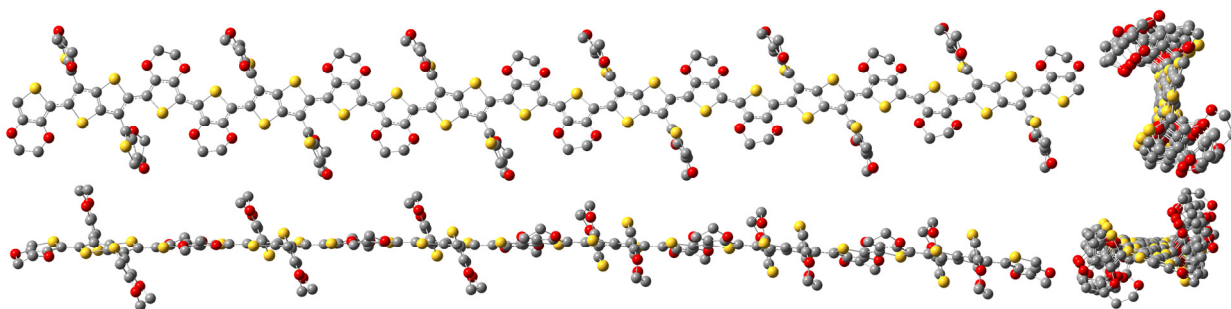
ΔE (helix–planar) = **-16.67 kJ/mol**

Fig. S4 B3LYP/6-31G(d) optimized geometries of helix and planar conformations of the hexamers **(CNPh-ETTE)₆** and **(Py-ETTE)₆**. Left pictures are the views perpendicular to the main chain and right pictures are the view along the main chain. Hydrogen atoms are omitted for clarity.

* *TT–EDOT* dihedrals between the end *TT* moieties and the neighboring inner *EDOT* units (at both sides) of **(CNPh-ETTE)₆ / planar** were frozen at $+10.5^\circ/-10.5^\circ$; rest coordinates were free to optimize.

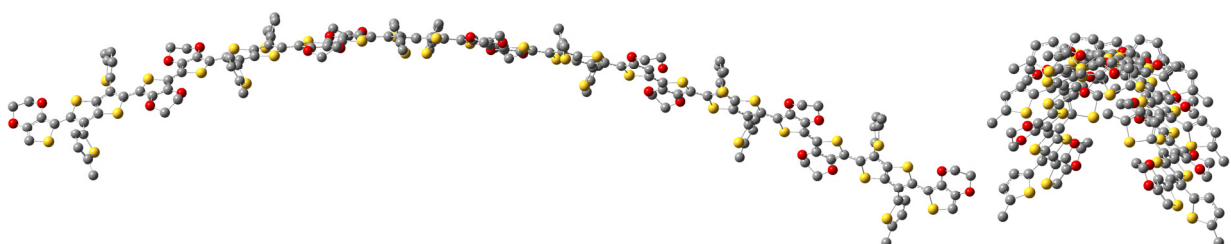


(EDOT-ETTE)₆ / helix (cis 3,6-EDOT/EDOT), $E_{\text{total}} = -24870.0852351$ Hartree

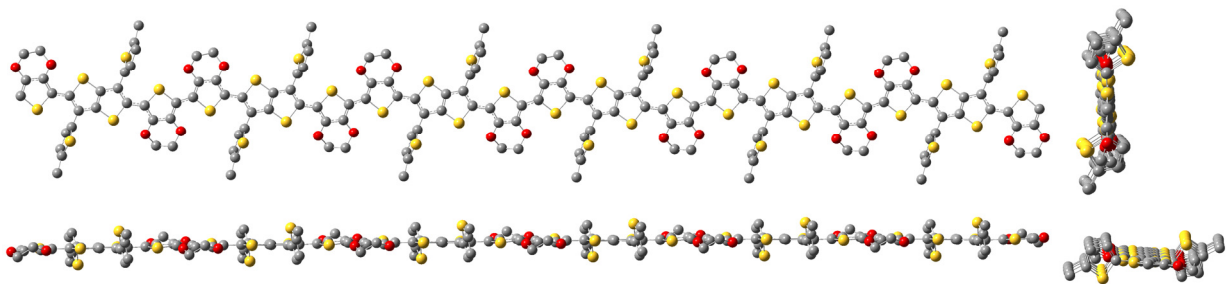


(EDOT-ETTE)₆ / planar (trans 3,6-EDOT/EDOT), $E_{\text{total}} = -24870.0863923$ Hartree

ΔE (helix–planar) = +3.04 kJ/mol



(MeTh-ETTE)₆ / helix (cis 3,6-MeTh/MeTh), $E_{\text{total}} = -22607.8508539$ Hartree



(MeTh-ETTE)₆ / planar (trans 3,6-MeTh/MeTh), $E_{\text{total}} = -22607.8496337$ Hartree*

ΔE (helix–planar) = –3.20 kJ/mol

Fig. S5 B3LYP/6-31G(d) optimized geometries of helix and planar conformations of the hexamers **(EDOT-ETTE)₆** and **(MeTh-ETTE)₆**. Left pictures are the views perpendicular to the main chain and right pictures are the view along the main chain. Hydrogen atoms are omitted for clarity.

* *Dihedrals at the EDOT–TT–EDOT along the backbone were frozen at +5°/–5° (except at the end monomer units, where dihedrals were free to optimize); two dihedrals TT–ThMe (end TT units, second MeTh groups from the ends of the molecule) were frozen at +80°/–80°.*

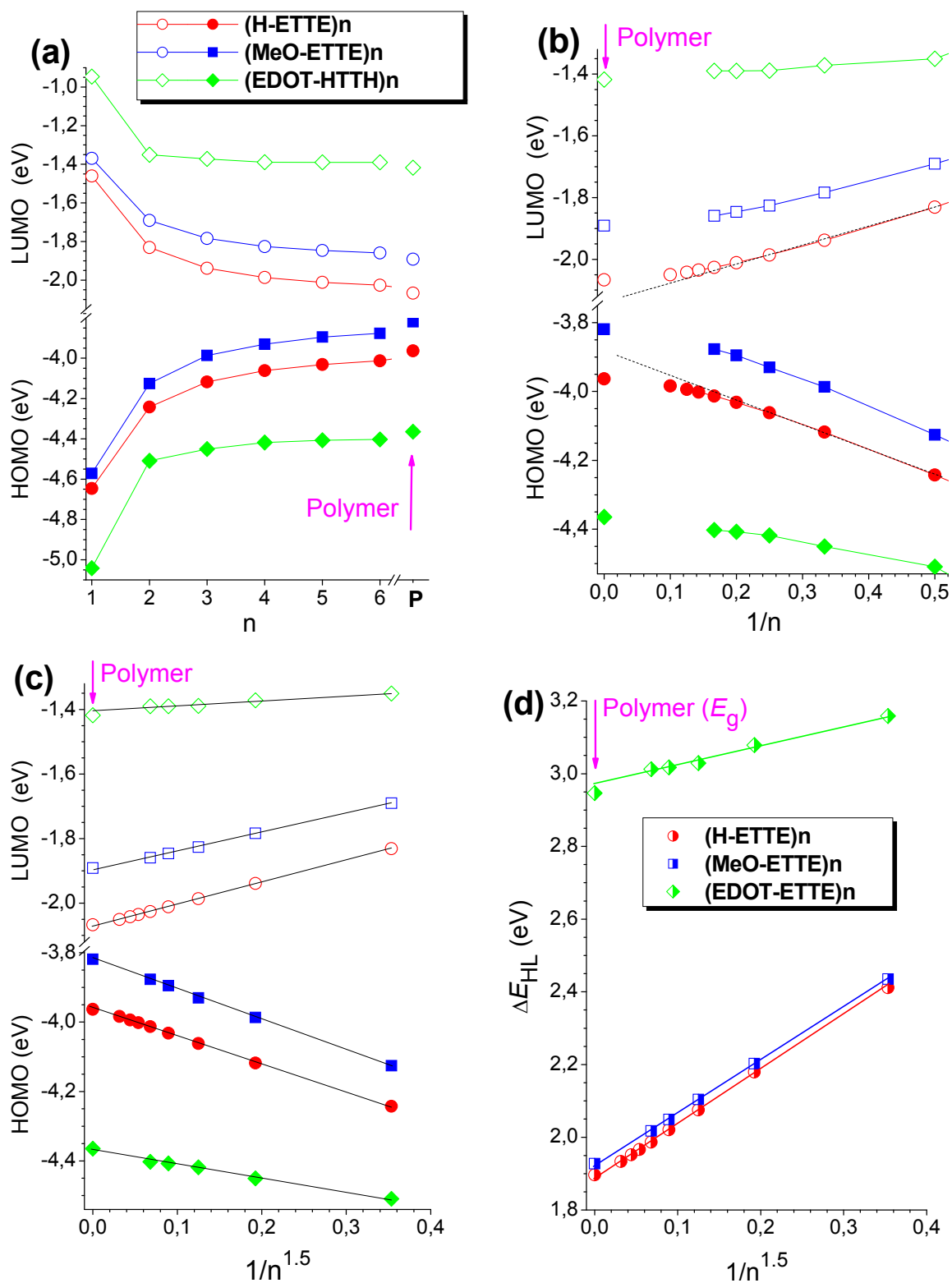


Fig. S6 Chain length dependences of HOMO/LUMO energies and the energy gaps for B3LYP/6-31G(d) optimized geometries of (H-ETTE)_n, (MeO-ETTE)_n and helix (EDOT-HTTH)_n oligomers and data for corresponding polymers P(H-ETTE), P(MeO-ETTE) and P(EDOT-HTTH) (by PBC):

HOMO and LUMO versus n (a), $1/n$ (b) and $1/n^{1.5}$ (c); energy gaps versus $1/n^{1.5}$ (d).

Dashed lines on graph (b) are to show that for long oligomers (i.e. at high n), the dependences of energies versus $1/n$ deviate from the linearity. However, for studied oligomers, excellent linear dependences were observed when empirical parameter $1/n^{1.5}$ was used [figures (c) and d)].

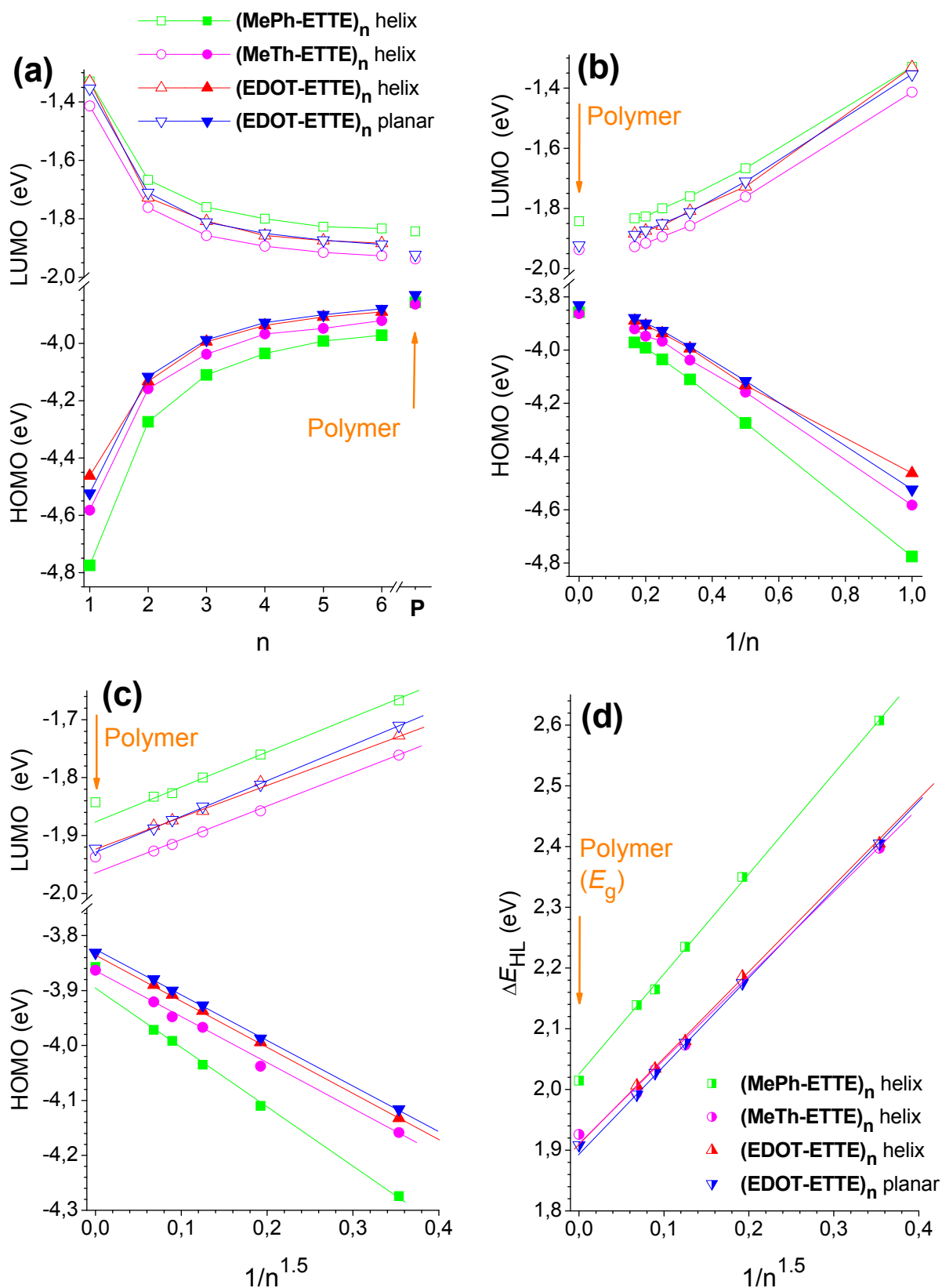


Fig. S7 Chain length dependences of HOMO/LUMO energies and the energy gaps for B3LYP/6-31G(d) optimized geometries of $(\text{MePh-ETTE})_n$, $(\text{MeTh-ETTE})_n$ and $(\text{EDOT-ETTE})_n$ oligomers and data for corresponding polymers $\text{P}(\text{MePh-ETTE})$, $\text{P}(\text{MeTh-ETTE})$ and $\text{P}(\text{EDOT-ETTE})$ (by PBC): HOMO and LUMO versus n (a), versus $1/n$ (b) and versus $1/n^{1.5}$ (c); ΔE_{HL} energy gaps versus $1/n^{1.5}$ (d). Linear correlations “ E vs $1/n^{1.5}$ ” are given in Table S2.

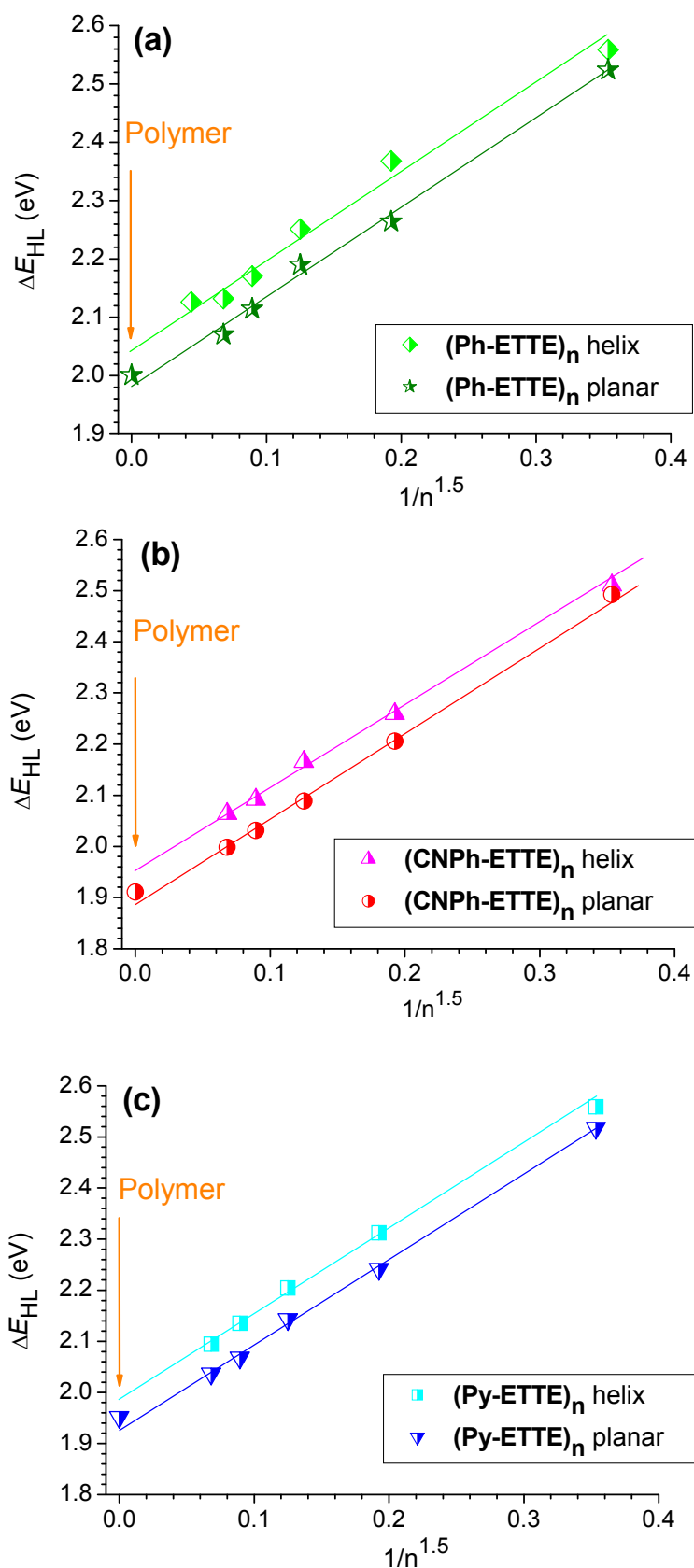


Fig. S8 Chain length dependences of the HOMO–LUMO energy gaps, ΔE_{HL} , versus $1/n^{1.5}$ for B3LYP/6-31G(d) optimized geometries of helix and planar conformations of: (a) **(Ph-ETTE)_n**, (b) **(Py-ETTE)_n** and (c) **(CNPh-ETTE)_n** oligomers. Band gaps (E_g) for corresponding polymers **P(Ph-ETTE)**, **P(Py-ETTE)** and **P(CNPh-ETTE)** (points at $1/n^{1.5}$) are from PBC calculations.

Table S1 Absolute energies, dihedral angles in the main chain and with the side groups, HOMO and LUMO energies and the HOMO-LUMO energy gaps for B3LYP/6-31G(d) optimized hexamers.

Hexamer [conformation]	E_{total} (Hartree) ^b	Main chain dihedrals EDOT-TT-EDOT	Side dihedrals (3,6-R)-TT	HOMO (eV)	LUMO (eV)	ΔE_{HL} , (eV)
(H-ETTE) ₆	-15514.3469487	1-3°	-	-4.01	-2.03	1.99
(MeO-ETTE) ₆	-16888.5374032	3-5°	-	-3.88	-1.86	2.02
(EDOT-HTTH) ₆ helix	-15514.3102867 [-5.03 kJ/mol]	14-16	-	-4.40	-1.39	3.01
(EDOT-HTTH) ₆ planar	-15514.30837	frozen at +9.0°/-9.0°	-	-4.38	-1.41	3.03
(EDOT-ETTE) ₆ helix (cis) ^a	-24870.0852351 [+3.04 kJ/mol]	9-14°	61-64°	-3.89	-1.88	2.01
(EDOT-ETTE) ₆ planar (trans) ^a	-24870.0863923	+4-6° -3-6°	+67-71° -65-73°	-3.88	-1.89	1.99
(MeTh-ETTE) ₆ helix (cis) ^a	-22607.8508539 [-3.20 kJ/mol]	6-11	64-71	-3.92	-1.93	1.99
(MeTh-ETTE) ₆ planar (trans) ^a	-22607.8496337	frozen at +5.0°/-5.0°	+90° -88°	-3.91	-1.91	2.01
(MePh-ETTE) ₆ helix	-18758.7842414	20-26°	53-56°	-3.97	-1.83	2.14
(Ph-ETTE) ₆ helix	-18286.9670284 [-15.76 kJ/mol]	19-25	55-58	-4.02	-1.89	2.13
(Ph-ETTE) ₆ planar	-18286.9610271	+14-16° -13-16°	+63-64° -63-65°	-3.94	-1.87	2.07
(CN-ETTE) ₆ helix	-19393.9004055 [-15.43 kJ/mol]	19-25°	52-56°	-4.60	-2.54	2.06
(CN-ETTE) ₆ planar	-19393.8945301	+10-11° -10-11°	+65-66° -65-66°	-4.47	-2.47	2.00
(Py-ETTE) ₆ helix	-18479.4111434 [-16.67 kJ/mol]	19-25	52-55	-4.37	-2.27	2.09
(Py-ETTE) ₆ planar	-18479.4047967	+13-14° -13-14°	+58-63° -62-66°	-4.27	-2.24	2.04

^a "cis" and "trans" belong to the orientation of S atoms of two thiophene side groups (in 3,6-positions) with respect to the plane of the backbone.

^b Differences in absolute energies of two conformers [$E_{\text{total}}(\text{helix}) - E_{\text{total}}(\text{planar})$] are shown in brackets.

Table S2 Comparison of PBC/B3LYP/6-31G(d) calculated HOCO, LUCO and E_g energies for polymers with extrapolated HOMO, LUMO and ΔE_{HL} energies from B3LYP/6-31G(d) calculations of the oligomers ($n = 2-6$)^a to the infinite chain length by linear correlations “ E vs $1/n^{1.5}$ ”.

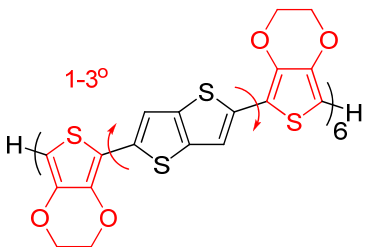
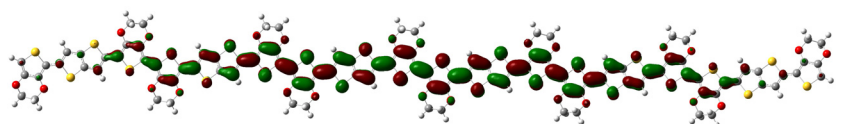
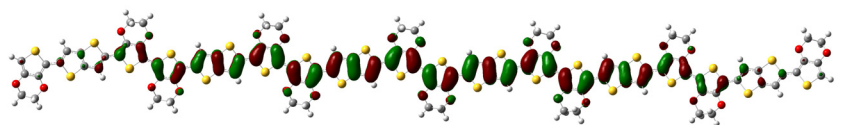
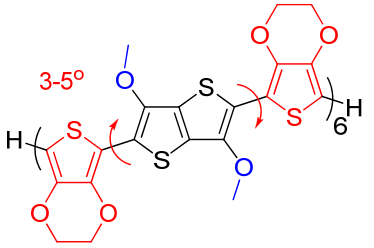
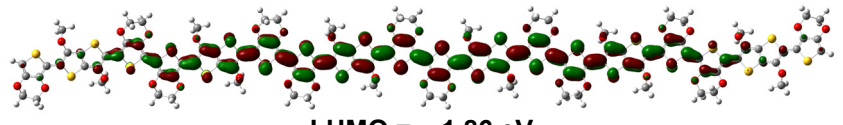
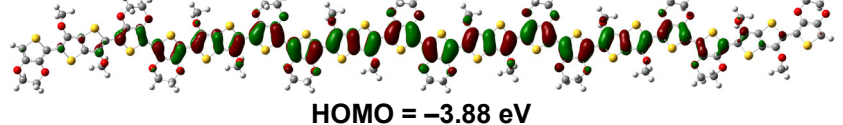
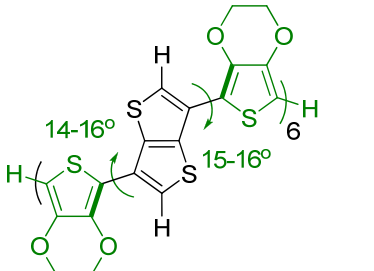
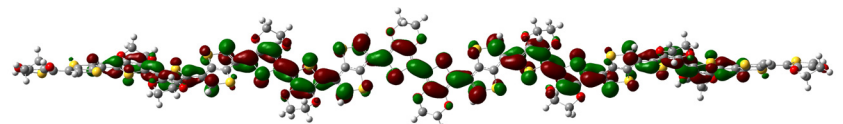
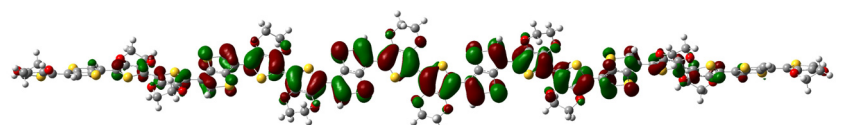
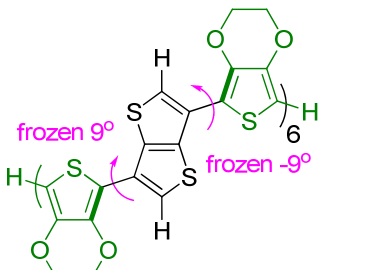
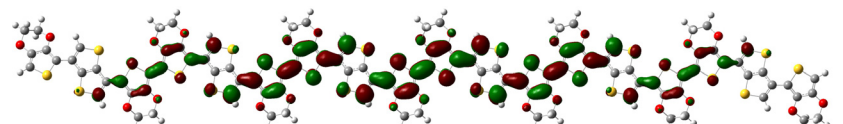
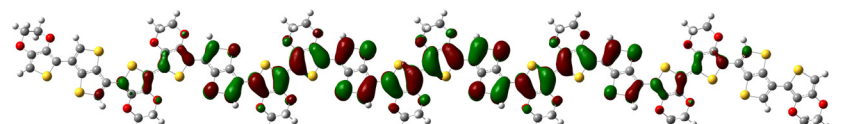
Polymer	Method	HOCO (HOMO), eV	LUCO (LUMO), eV	E_g (ΔE_{HL}), eV
P(H-ETTE)	PBC ^b oligomer ^c	-3.963 -3.959±0.001	-2.067 -2.072±0.001	1.897 1.887±0.001
P(MeO-ETTE)	PBC oligomer	-3.819 -3.819±0.002	-1.891 -1.899±0.001	1.928 1.919± 0.002
P(EDOT-HTTH)	PBC oligomer (planar) oligomer (helix)	-4.364 - -4.374±0.003	-1.418 - -1.403±0.003	2.947 - 2.971±0.005
P(EDOT-ETTE)	PBC oligomer (planar) oligomer (helix)	-3.831 - -3.831±0.001	-1.923 - -1.922±0.006	1.908 - 1.909±0.006
P(MeTh-ETTE)	PBC oligomer (planar) oligomer (helix)	-3.863 - -3.869±0.006	-1.937 - -1.967±0.001	1.926 - 1.902±0.005
P(MePh-ETTE)	PBC oligomer (planar) oligomer (helix)	-3.857 - -3.911±0.022	-1.843 - -1.873±0.008	2.014 - 2.038±0.030
P(Ph-ETTE)	PBC oligomer (planar) oligomer (helix)	-3.899 -3.901±0.008 -3.974±0.018	-1.898 -1.908±0.005 -1.924±0.004	2.001 1.992±0.012 2.050±0.022
P(CNPh-ETTE)	PBC oligomer (planar) oligomer (helix)	-4.420 -4.410±0.002 -4.544±0.003	-2.509 -2.534±0.0048 -2.585±0.003	1.911 1.875±0.004 1.959±0.006
P(Py-ETTE)	PBC oligomer (planar) oligomer (helix)	-4.212 -4.195±0.002 -4.307±0.006	-2.260 -2.272±0.005 -2.313±0.002	1.951 1.923±0.006 1.994±0.008

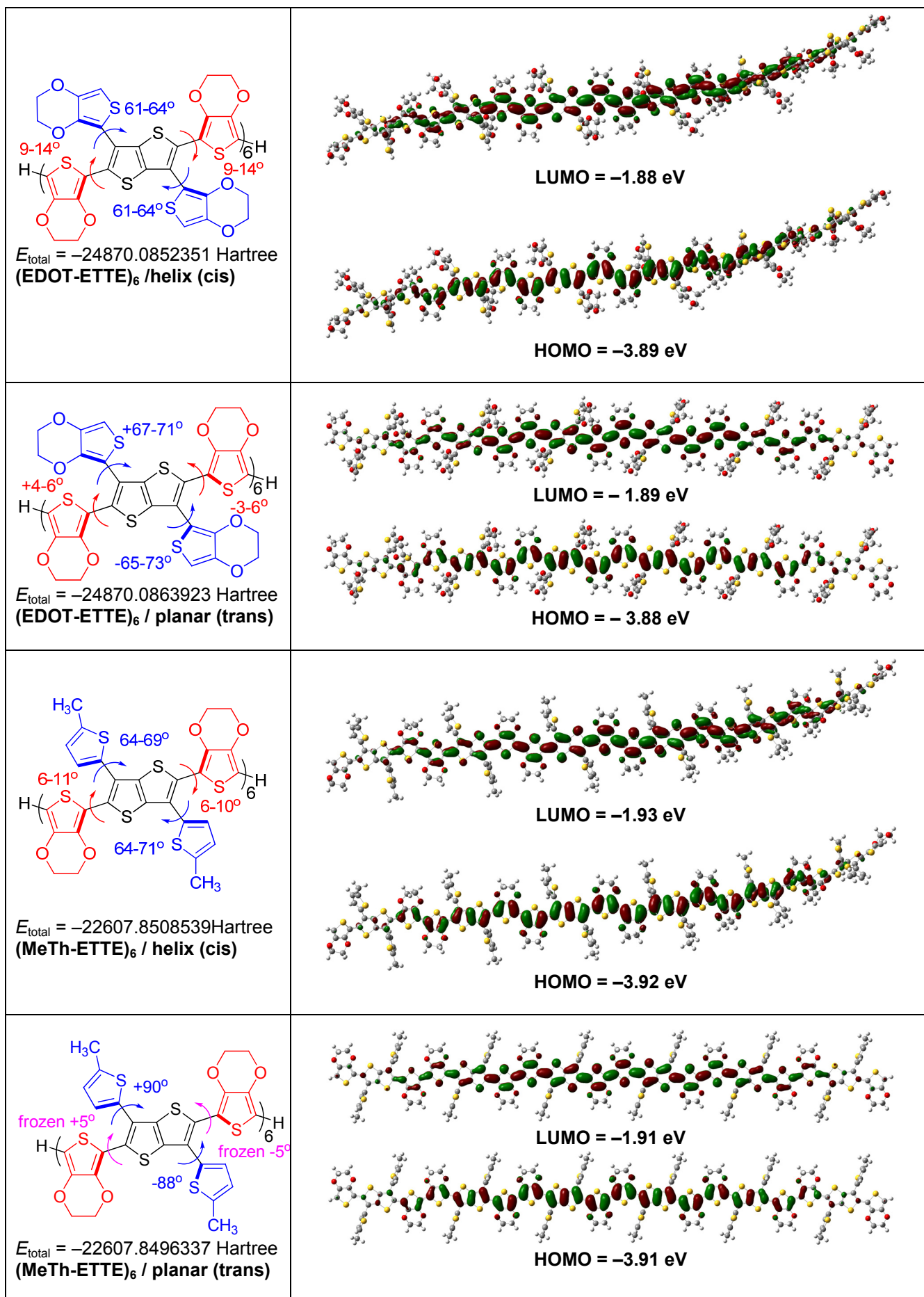
^a $n = 2-8, 10$ for **P(H-ETTE)**.

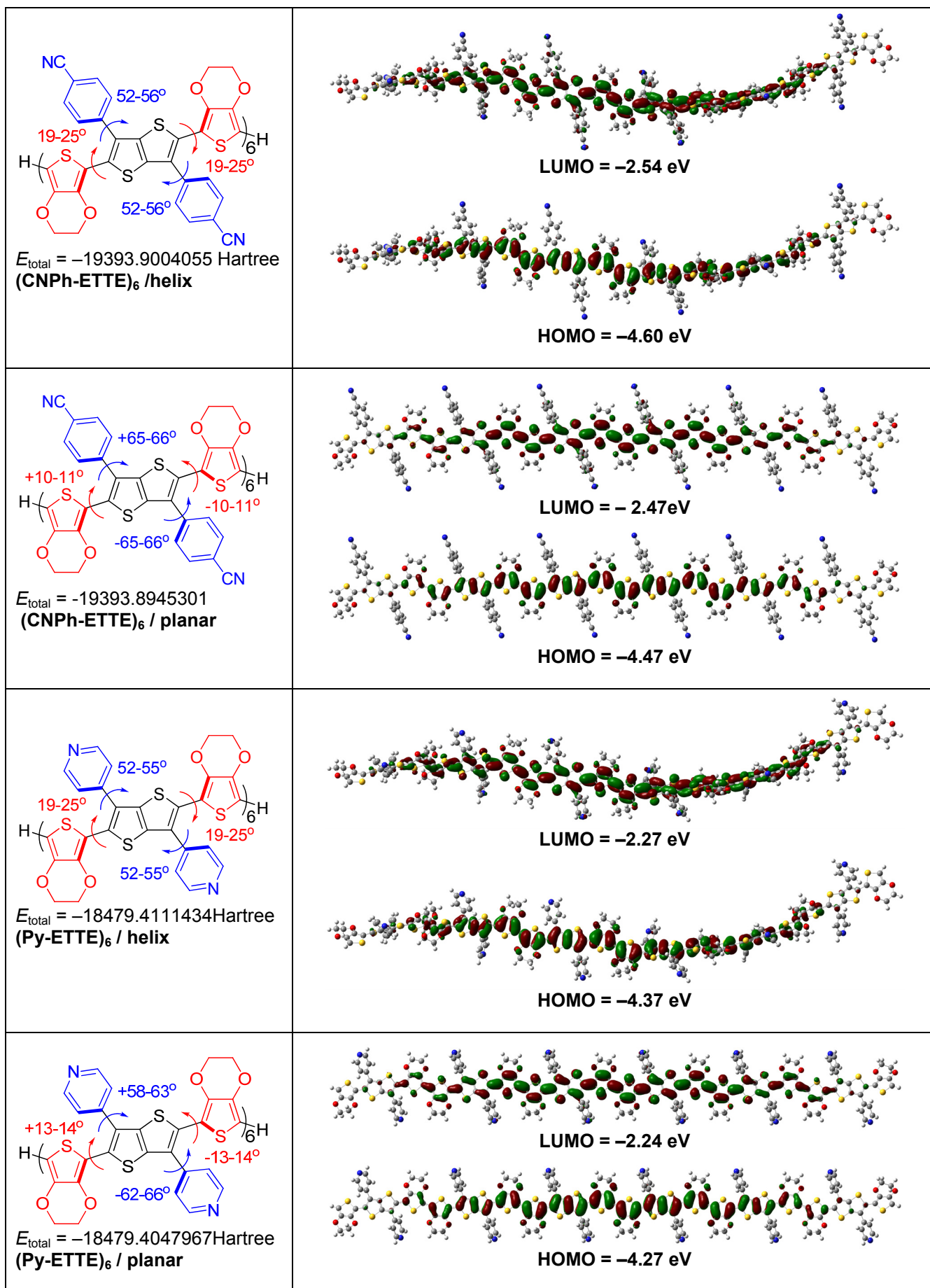
^b Calculations of polymers using periodic boundary conditions (PBC) formalism.

^c Calculations of polymers by extrapolation of linear dependences “ E vs $1/n^{1.5}$ ” for oligomers to the infinite chain length.

Fig. S9 (4 pages)

Structures of the hexamers	Distribution of HOMO/LUMO orbital densities (isovalue = 0.015) and HOMO/LUMO energy levels
 <p>$E_{\text{total}} = -15514.3469487$ Hartree (H-ETTE)₆ / planar</p>	 <p>LUMO = -2.03 eV</p>  <p>HOMO = -4.01 eV</p>
 <p>$E_{\text{total}} = -16888.5374032$ Hartree (MeO-ETTE)₆ / planar</p>	 <p>LUMO = -1.86 eV</p>  <p>HOMO = -3.88 eV</p>
 <p>$E_{\text{total}} = -15514.3102867$ Hartree (EDOT-HTTH)₆ / helix</p>	 <p>LUMO = -1.39 eV</p>  <p>HOMO = -4.40 eV</p>
 <p>$E_{\text{total}} = -15514.30837$ Hartree (EDOT-HTTH)₆ / planar</p>	 <p>LUMO = -1.41 eV</p>  <p>HOMO = -4.38 eV</p>





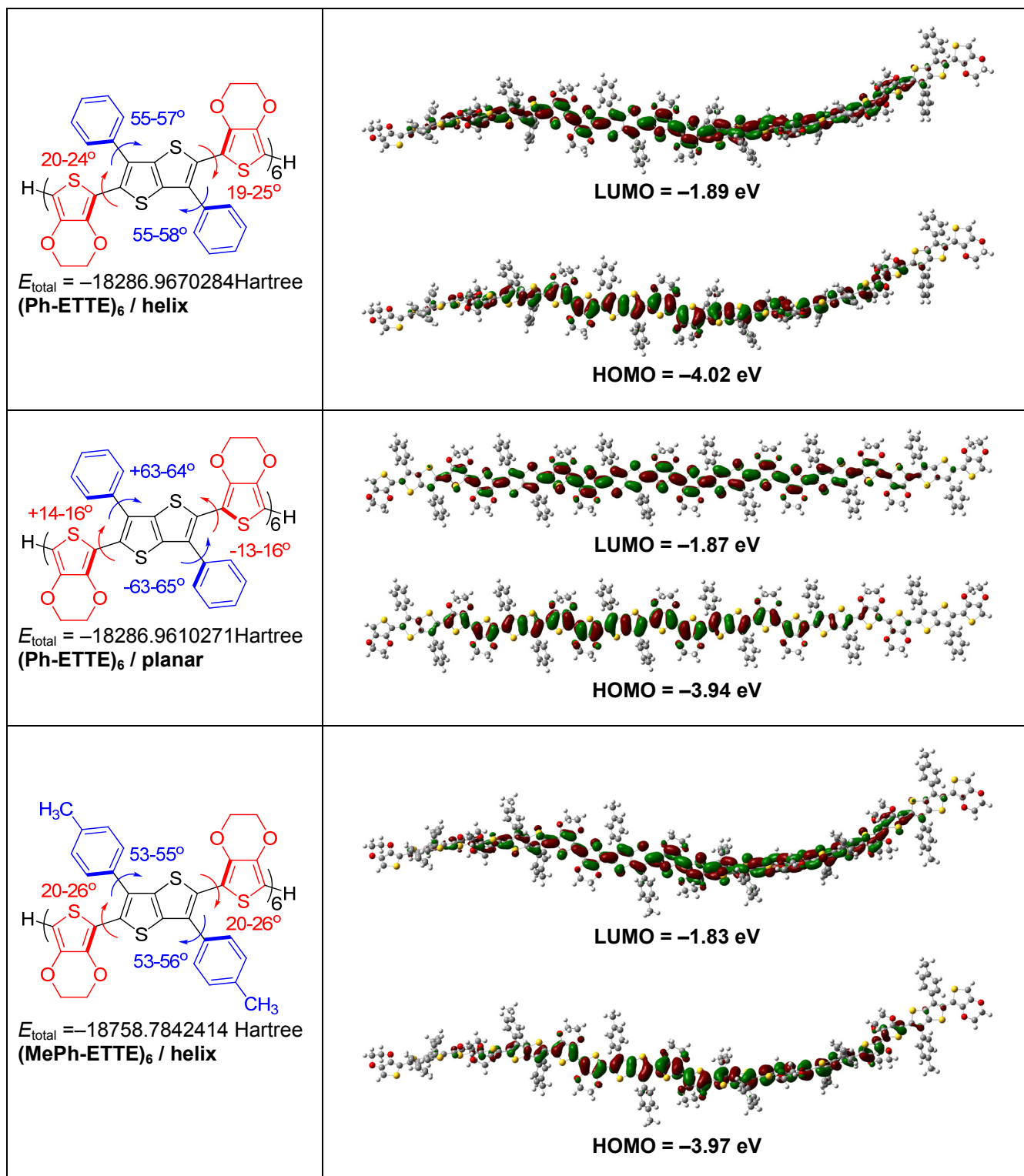


Fig. S9 The absolute energies of B3LYP/6-31G(d) optimized geometries of the hexamers **(R-ETTE)₆** and **(EDOT-HTTH)₆**, the TT-EDOT dihedral angles in the main chain and R-TT dihedral angles with the side groups, the HOMO and LUMO orbital energies and the contour plots of the frontier orbital densities in the molecules.

The arrows on the formulas show the direction of the rotation of 2,5-EDOT and 3,6-R substituents with respect to the central TT moiety (dihedral angles at the end TT-EDOT moieties were not taken into account). The positive sign means clockwise rotation when viewing from the TT side to the 2,5-EDOTs or 3,6-R groups, the negative sign means anticlockwise rotation.

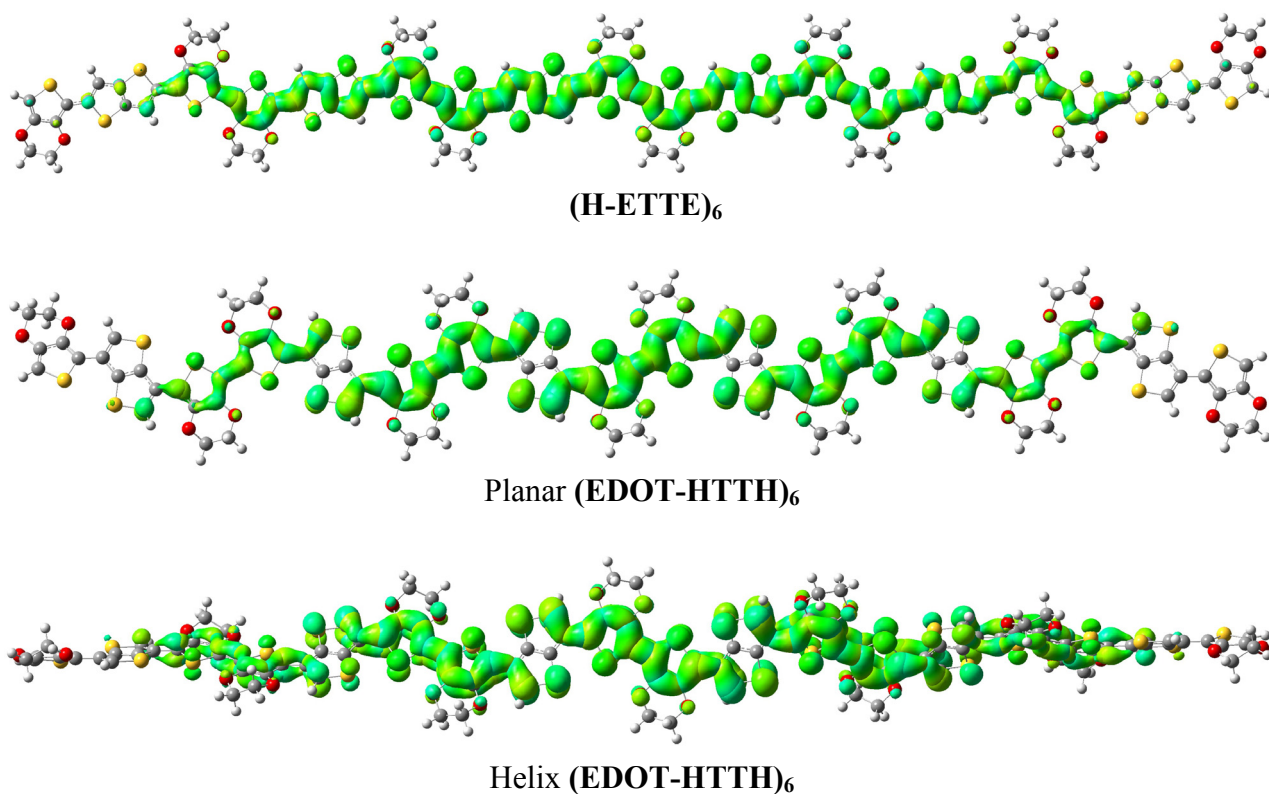
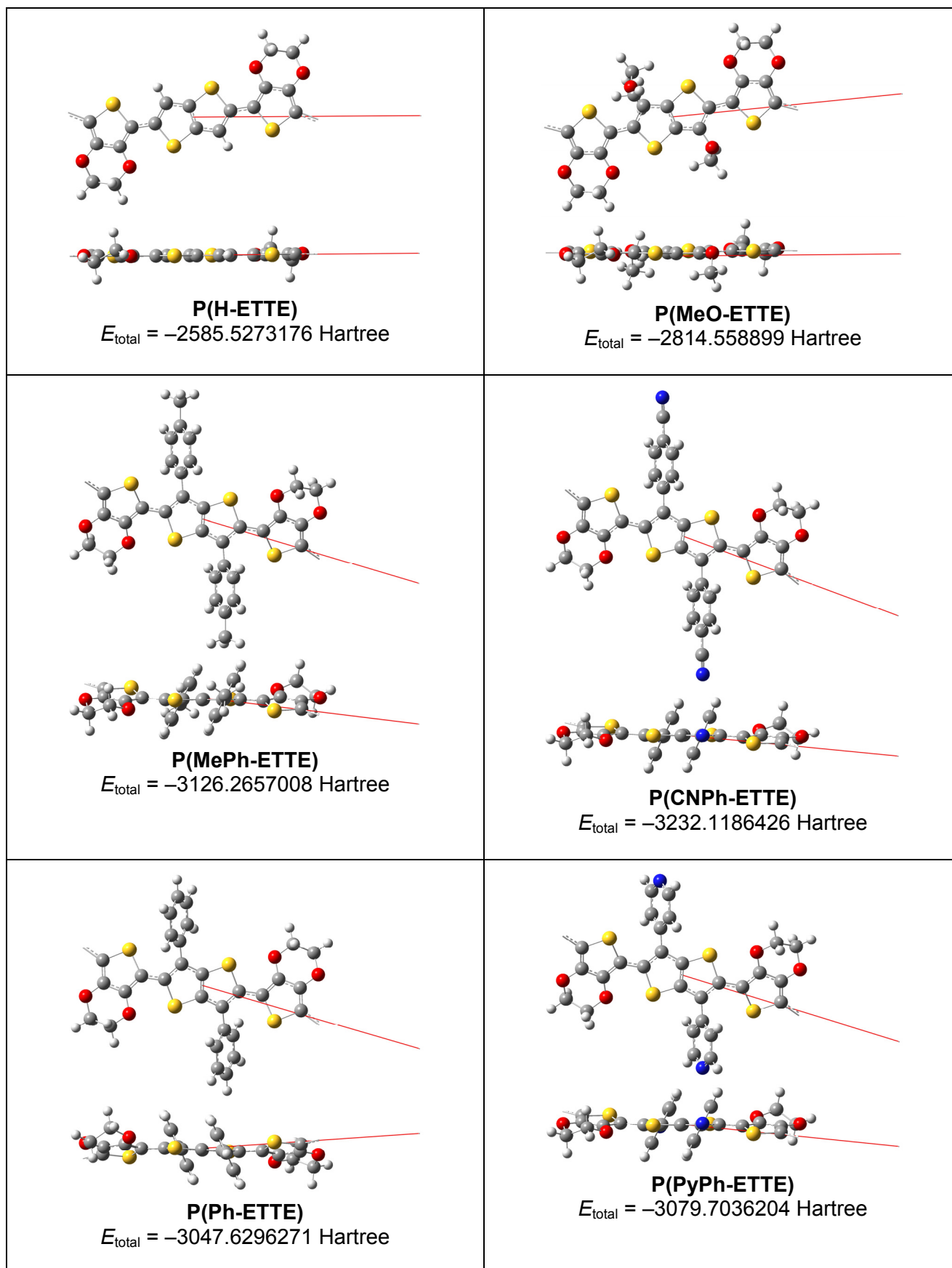


Fig. S10 Mapped orbital surfaces of (HOMO+LUMO) for **(H-ETTE)₆** and **(EDOT-HTTH)₆** (planar and helix conformations).

It is clear seen the differences in the frontier orbitals distribution in these two hexamers. In contrast to **(H-ETTE)₆** which show high degree of conjugation with long-range HOMO/LUMO orbitals delocalization along the backbone, in the case of **(EDOT-HTTH)₆** hexamer, there is no frontier orbital coefficients at the central C=C bonds of the TT moiety. Consequently, the conjugation in both the helix and planar conformations of **(EDOT-HTTH)₆** is only extended on the two EDOTs and two halves of the TT moieties.

B3LYP/6-31G(d) calculations for polymers by PBC.

Fig. S11 (2 pages)



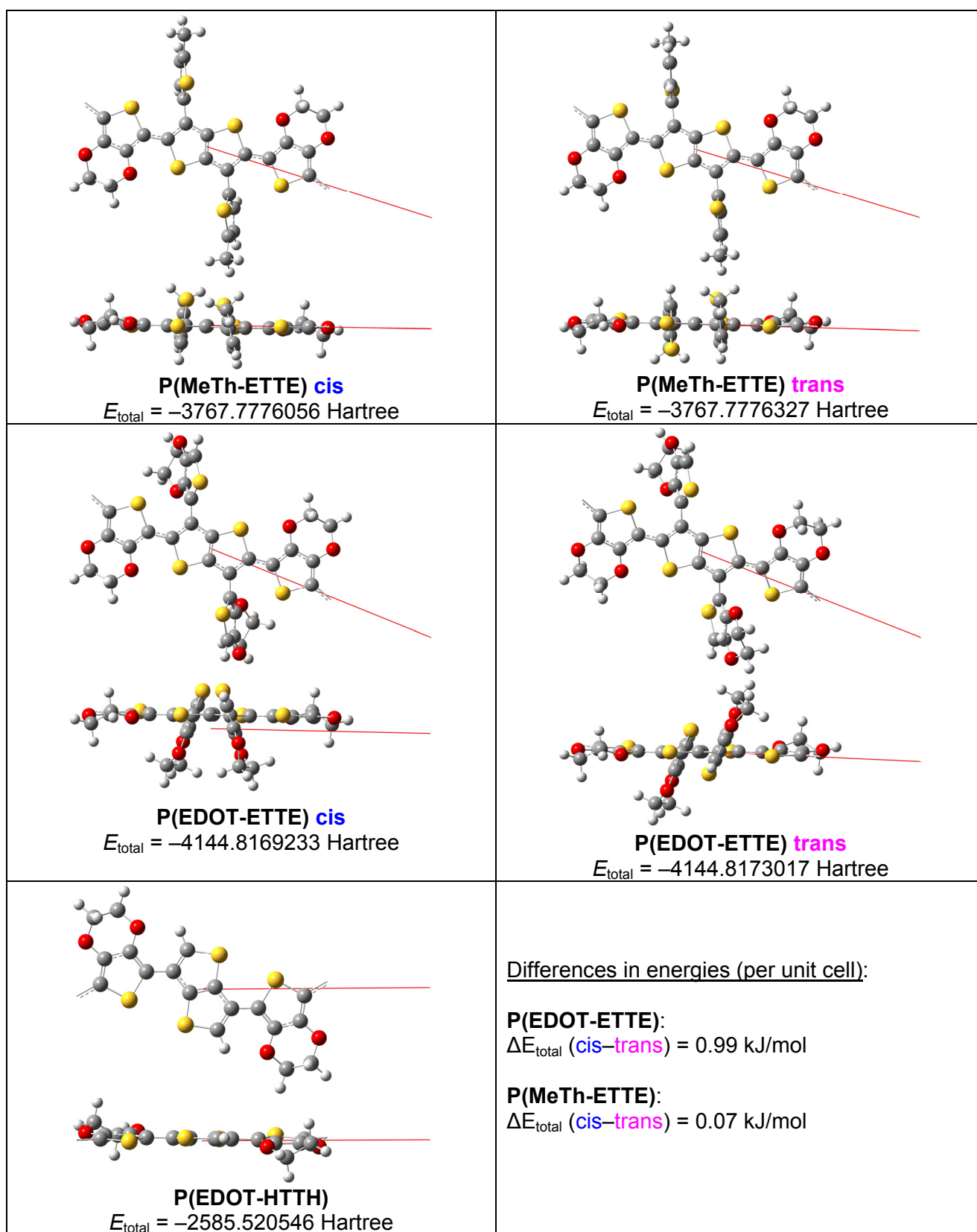
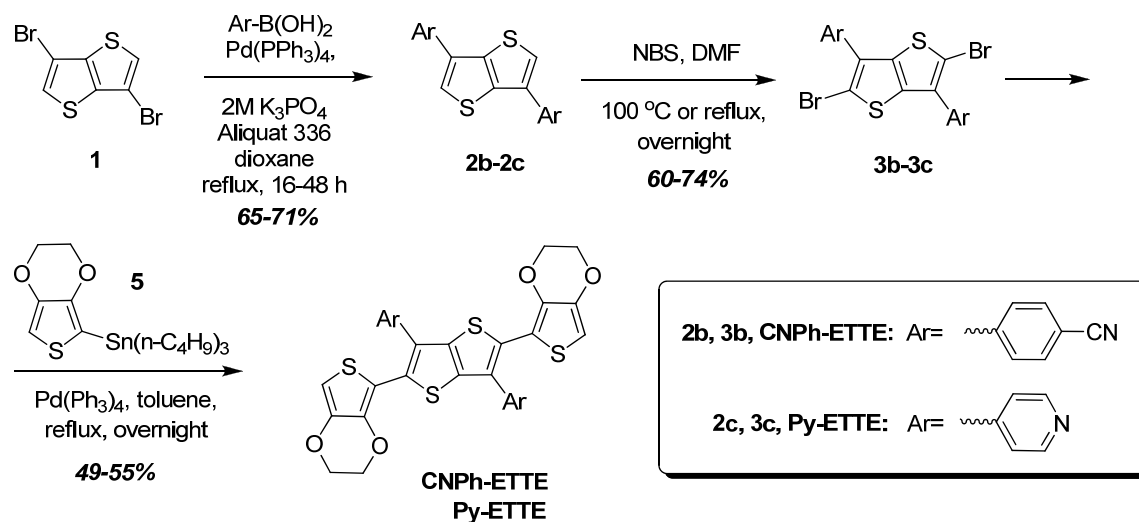


Fig. S11. Unit cells for the optimized structures of **P(R-ETTE)** and **P(EDOT-HTTH)** polymers calculated at PBC/B3LYP/6-31G(d). Top and side views are shown for each polymer. Absolute energies (E_{total}) are per unit cells. For **P(EDOT-ETTE)** and **P(MeTh-ETTE)**, two conformations have been calculated, i.e. with S atoms of the side thiophene rings on the same side (**cis**) and on the opposite sides (**trans**) of the polymer backbone. Both conformations have very similar energies, while the trans-isomers are slightly more stable.

Synthesis

Synthetic route to CNPh-ETTE and Py-ETTE:



4,4'-(thieno[3,2-*b*]thiophene-3,6-diyl)dibenzonitrile (**2b**).

To the solution of 3,6-dibromothiopheno[3,2-*b*]thiophene (**1**) (4.43 g, 15 mmol) and 4-cyanophenylboronic acid (6.61 g, 45 mmol) in dioxane (150 mL) 2M K₃PO₄ (90 mmol, 45 mL), Pd(PPh₃)₄ (0.34 g, 2 mol%) and Aliquat 336 (7.5 mol%) were added under N₂ atmosphere. The reaction mixture was refluxed for 16 h and cooled to room temperature. The precipitate was filtered off, dried *in vacuo* at 50 °C and the crude product was purified by sublimation to yield pure compound **2b** (3.64 g, 71%).

¹H NMR (300 MHz, CDCl₃): δ (ppm) 7.87 (d, *J* = 8.5 Hz, 4H), 7.79 (d, *J* = 8.5 Hz, 4H), 7.72 (s, 2H).

3,6-di(pyridin-4-yl)thieno[3,2-*b*]thiophene (**2c**).

To the solution of 3,6-dibromothiopheno[3,2-*b*]thiophene (**1**) (4.43 g, 15 mmol) and 4-pyridylboronic acid (5.54 g, 45 mmol) in dioxane (150 mL), 2M K₃PO₄ (90 mmol, 45 mL), Pd(PPh₃)₄ (0.34 g, 2 mol%) and Aliquat 336 (7.5 mol%) were added under N₂ atmosphere. The reaction mixture was refluxed for 48 h and cooled to room temperature. The precipitate was filtered off, dried *in vacuo* at 50 °C and the crude product was purified by sublimation to yield pure compound **2c** (2.82 g, 65%).

¹H NMR (400 MHz, CDCl₃): δ (ppm) 8.80–8.67 (m, 4H), 7.82 (s, 2H), 7.70–7.60 (m, 4H).

4,4'-(2,5-dibromothiopheno[3,2-*b*]thiophene-3,6-diyl)dibenzonitrile (**3b**).

To the solution of compound **2b** (3.05 g, 10 mmol) in *N,N*-dimethylformamide (150 mL), *N*-bromosuccinimide (7.00 g, 40 mmol) was added portionwise at 100 °C. The reaction mixture was stirred under reflux overnight and cooled to room temperature. The solid was filtered off, washed with saturated Na₂CO₃, three times with water and acetone, and dried *in vacuo* at 50 °C to afford compound **3b** (2.98 g, 60%).

¹H NMR (400 MHz, CDCl₃): δ (ppm) 7.82 (d, *J* = 8.7 Hz, 4H), 7.78 (d, *J* = 8.7 Hz, 4H), 7.52 (s, 2H).

4,4'-(2,5-dibromothieno[3,2-*b*]thiophene-3,6-diyl)dipyridine (3c).

To the solution of compound **2c** (2.95 g, 10 mmol) in *N,N*-dimethylformamide (150 mL), *N*-bromosuccinimide (7.00 g, 40 mmol) was added portionwise at 100 °C. The reaction mixture was heated at 100 °C overnight and cooled to room temperature. The solid was filtered off, washed with saturated Na₂CO₃, three times with water and acetone, and dried *in vacuo* at 50 °C to afford compound **3c** (3.33 g, 74%).

¹H NMR (400 MHz, CDCl₃): δ (ppm) 8.82–8.75 (m, 4H), 7.63–7.57 (m, 4H).

4,4'-(2,5-bis(2,3-dihydrothieno[3,4-*b*][1,4]dioxin-5-yl)thieno[3,2-*b*]thiophene-3,6-diyl)-dibenzonitrile (CNPh-ETTE).

4,4'-(2,5-dibromothieno[3,2-*b*]thiophene-3,6-diyl)dibenzonitrile (**2b**) (2.50 g, 5 mmol) and 2-tributylstannyl-3,4-ethylenedioxythiophene (**5**) (6.04 g, 14 mmol) were dissolved in anhydrous toluene (50 mL). The solution was purged with argon for 15 min and Pd(PPh₃)₄ (0.12 g, 0.1 mmol) was added at room temperature under argon atmosphere. The mixture was stirred at 120 °C under argon atmosphere for 24 h, cooled down to room temperature and quenched with water. The mixture was extracted with dichloromethane, the organic layer was dried over anhydrous MgSO₄, filtered off and the filtrate was evaporated on rotary evaporator to afford crude product. The crude product was purified by column chromatography (CH₂Cl₂:hexane, 2:1) to yield compound **CNPh-ETTE** (1.71 g, 55%) as brown-yellow solid.

¹H NMR (400 MHz, CDCl₃): δ (ppm) 7.72 (d, *J* = 8.5 Hz, 4H), 7.64 (d, *J* = 8.5 Hz, 4H), 6.34 (s, 2H), 4.17–1.09 (m, 4H), 4.07–3.98 (m, 4H).

HRMS (ESI+): *m/z* 623.0222 [M+H]⁺ (calcd for C₃₂H₁₉N₂O₄S₄ 623.0228).

4,4'-(2,5-bis(2,3-dihydrothieno[3,4-*b*][1,4]dioxin-5-yl)thieno[3,2-*b*]thiophene-3,6-diyl)-dipyridine (Py-ETTE).

4,4'-(2,5-dibromothieno[3,2-*b*]thiophene-3,6-diyl)dipyridine (**2c**) (2.25 g, 5 mmol) and 2-tributylstannyl-3,4-ethylenedioxythiophene (**5**) (6.04 g, 14 mmol) were dissolved in anhydrous toluene (50 mL). The solution was purged with argon for 15 min and Pd(PPh₃)₄ (0.12 g, 0.1 mmol) was added at room temperature under argon atmosphere. The mixture was stirred at 120 °C under argon atmosphere for 24 h, cooled down to room temperature and quenched with water. The mixture was extracted with dichloromethane, the organic layer was dried over anhydrous MgSO₄, filtered off and the filtrate was evaporated on rotary evaporator to afford crude product. The crude product was purified by column chromatography (CH₂Cl₂:hexane, 1:1) to yield compound **Py-ETTE** (1.41 g, 49%) as brown-yellow solid.

¹H NMR (400 MHz, CDCl₃) δ (ppm): 8.70–8.62 (m, 4H), 7.48–7.41 (m, 4H), 6.37 (s, 2H), 4.15–4.08 (m, 4H), 4.03–3.97 (m, 4H).

HRMS (+ESI) (*m/z*): 575.0222 [M+H] (calcd for C₂₈H₁₉N₂O₄S₄ 575.0228).

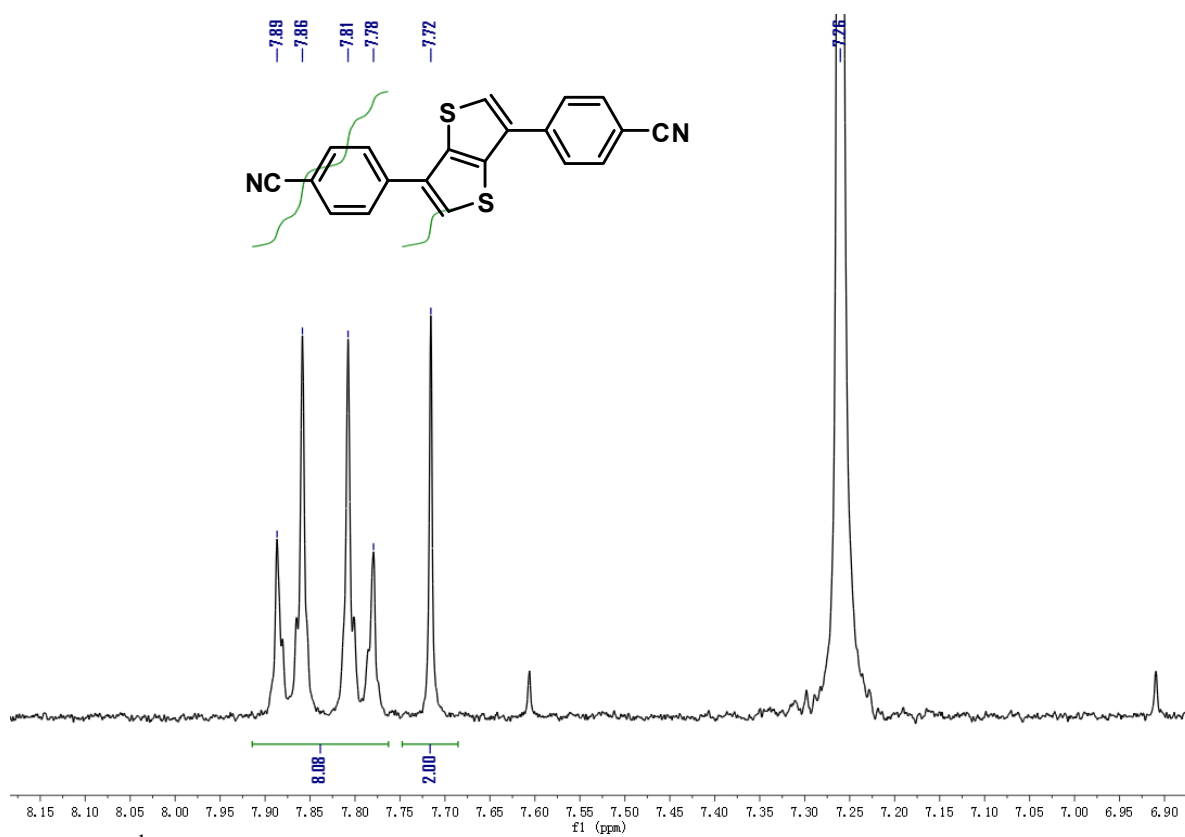


Fig. S12 ¹H NMR spectrum of compound **2b**.

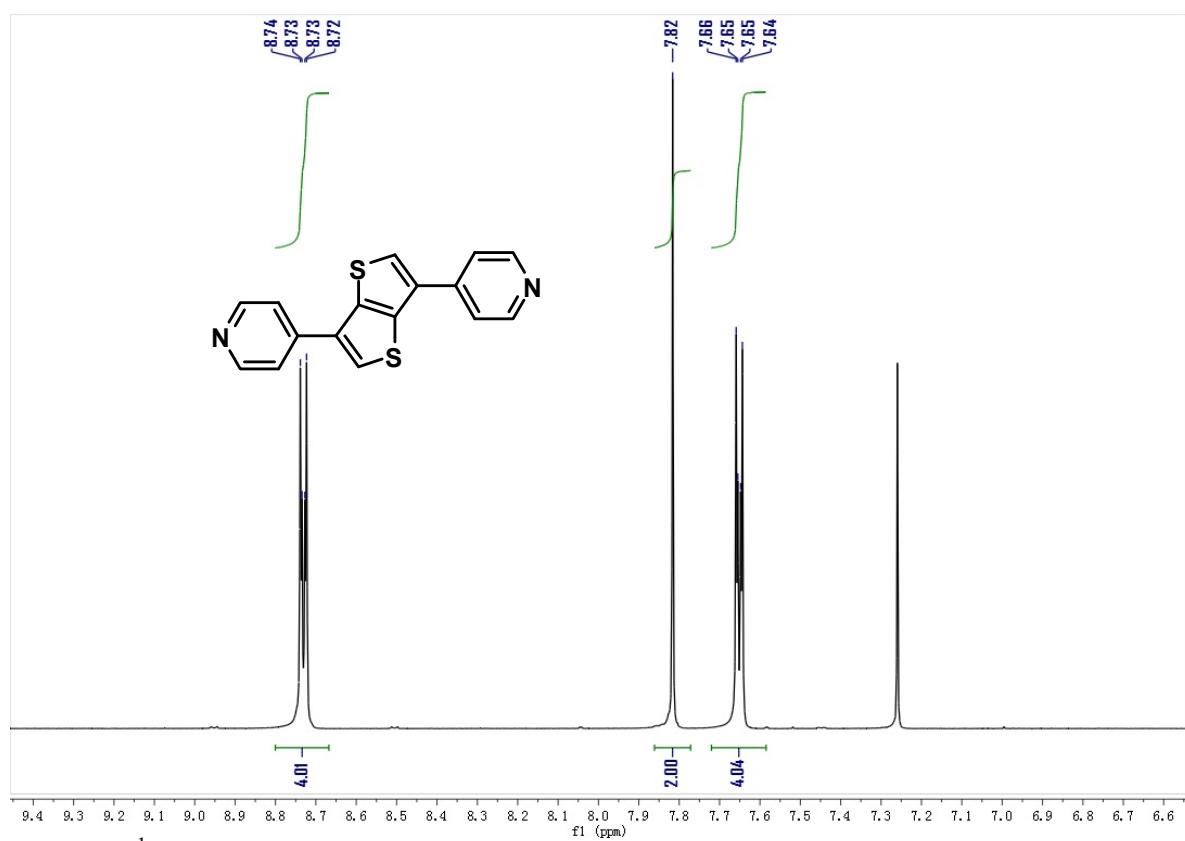


Fig. S13 ¹H NMR spectrum of compound **2c**.

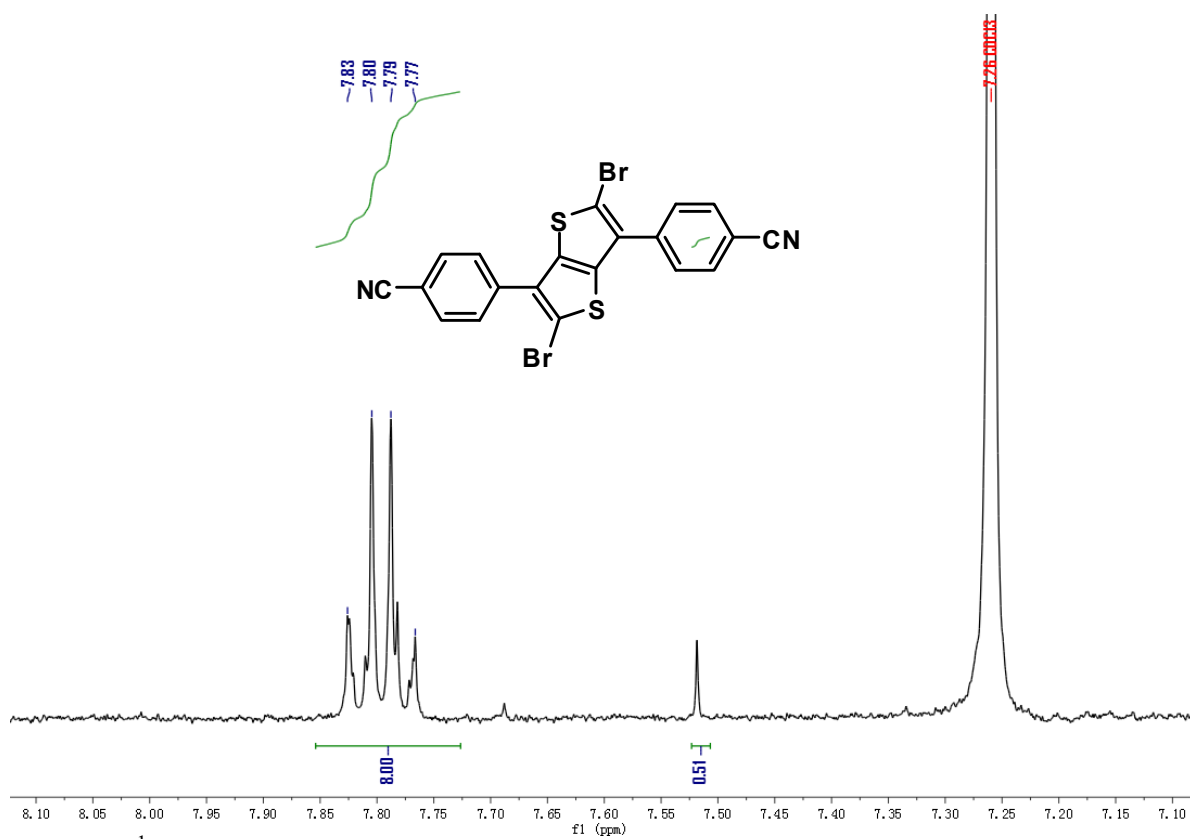


Fig. S14 ^1H NMR spectrum of compound 3b.

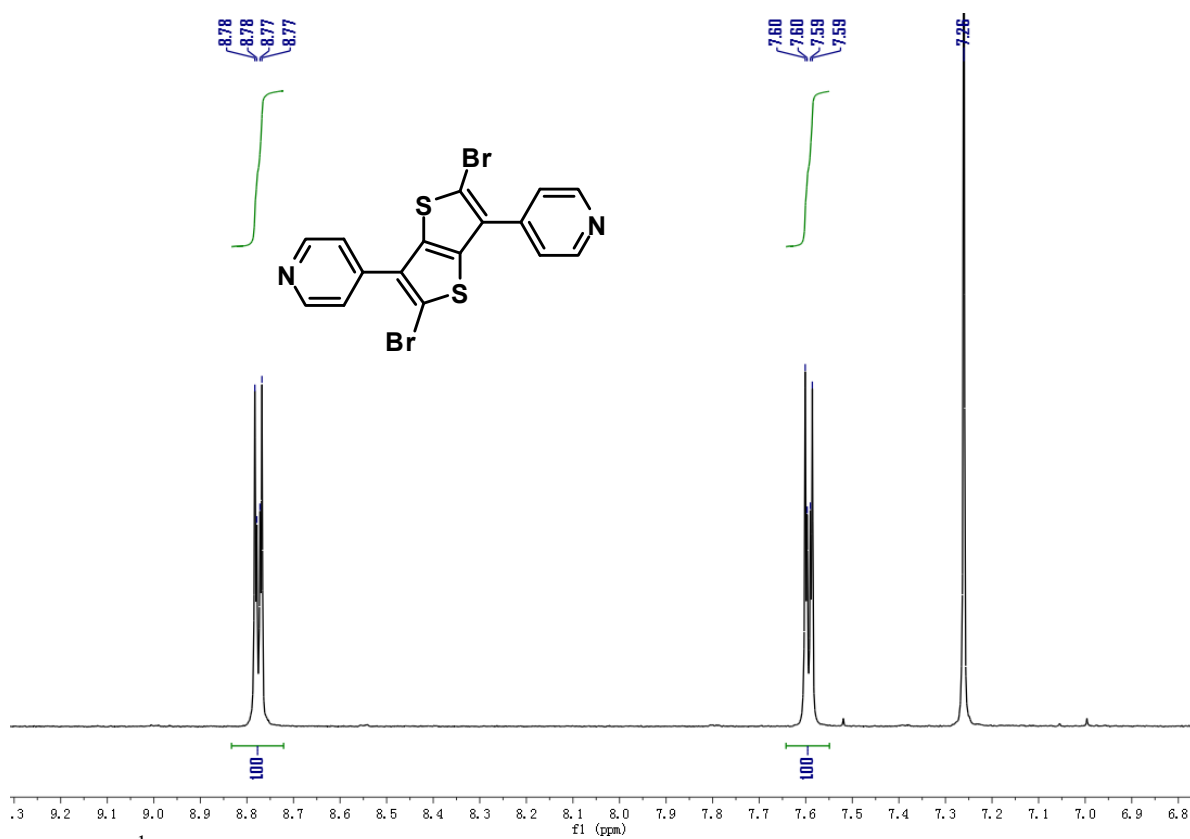


Fig. S15 ^1H NMR spectrum of compound 3c.

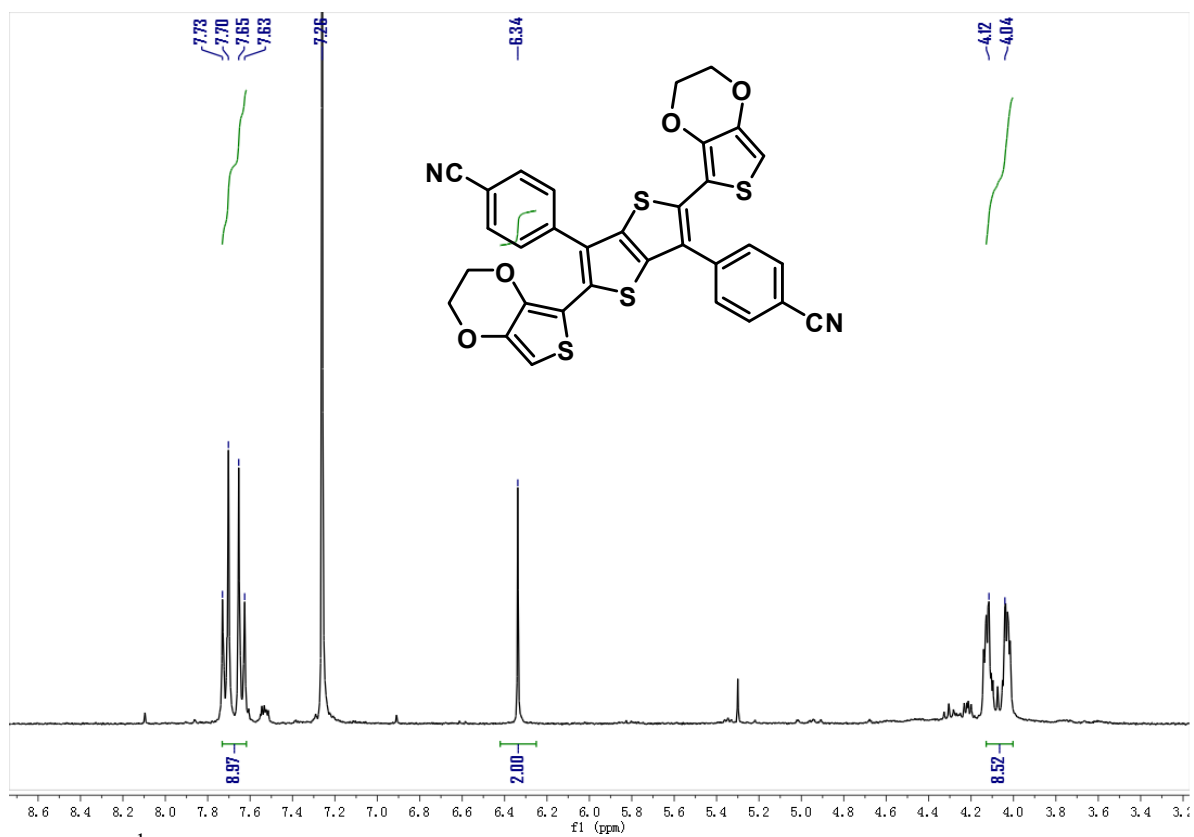


Fig. S16 ^1H NMR spectrum of compound CNPh-ETTE.

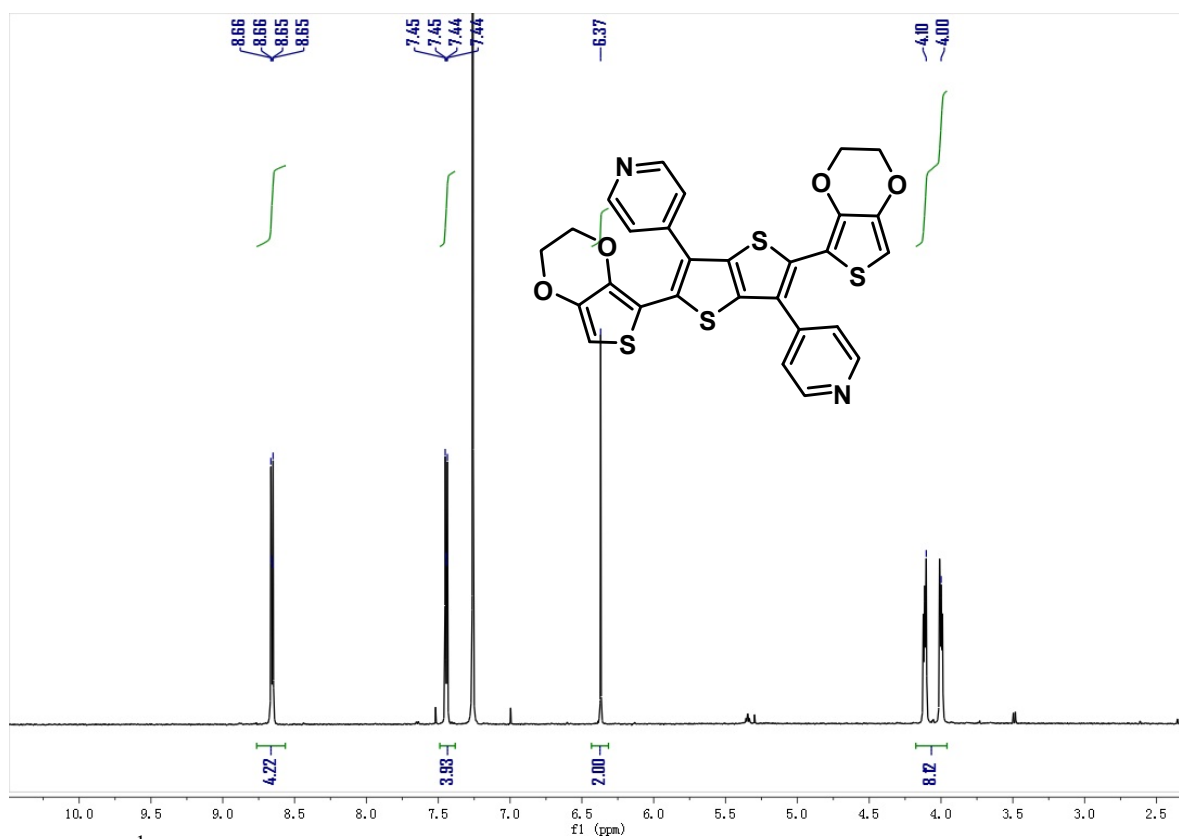


Fig. S17 ^1H NMR spectrum of compound Py-ETTE.

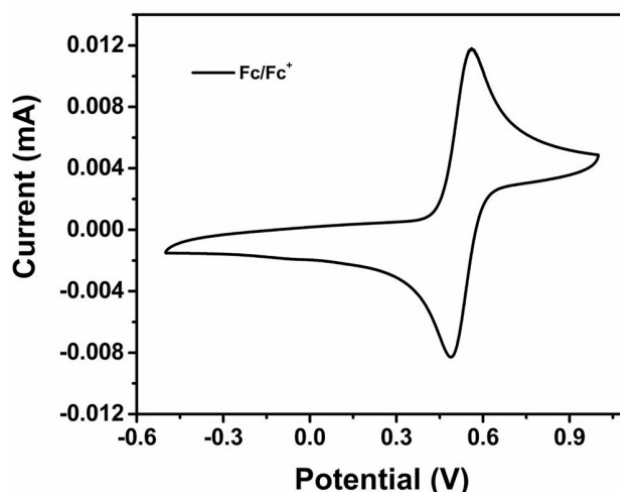


Fig. S18 Cyclic voltammogram of Fc/Fc^+ versus Ag wire pseudo-reference electrode in $\text{ACN}/\text{TBAPF}_6$ (0.1 M) solution at 100 mV/s under nitrogen atmosphere.

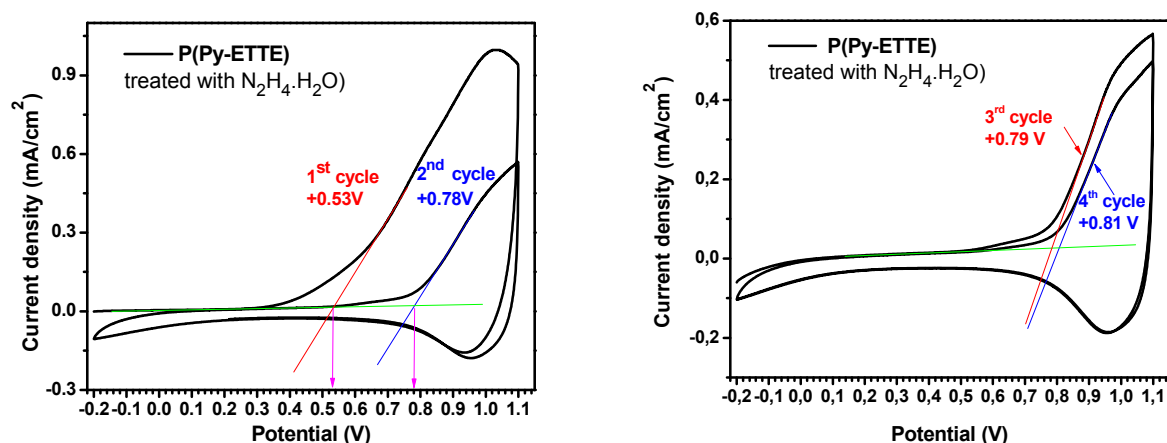


Fig. S19 Cyclic voltammogram of **P(Py-ETTE)** films treated with hydrazine hydrate solution in ACN ; $\text{ACN}/\text{TBAPF}_6$ (0.1 M), 100 mV/s.

***Procedure:** After normal electropolymerization of **Py-ETTE**, the **P(Py-ETTE)** polymer film was placed into the 5% solution of hydrazine hydrate in ACN for about 1 h to deprotonate/dedope the polymer. After that, the polymer film was carefully rinsed 3 times with fresh ACN and its CV was measured. The results indicate that such deprotonated/dedoped film show substantially lower oxidation potential of +0.53 V on the 1st cycle which, however, is anodically shifted on cycling to the initial value of +0.83 V, obtained for the “as prepared” **P(Py-ETTE)** film. This might indicate that initially deprotonated/dedoped polymer undergoes partial protonation during anodic cycling from traces of water to be present in the film (or in the solvent).

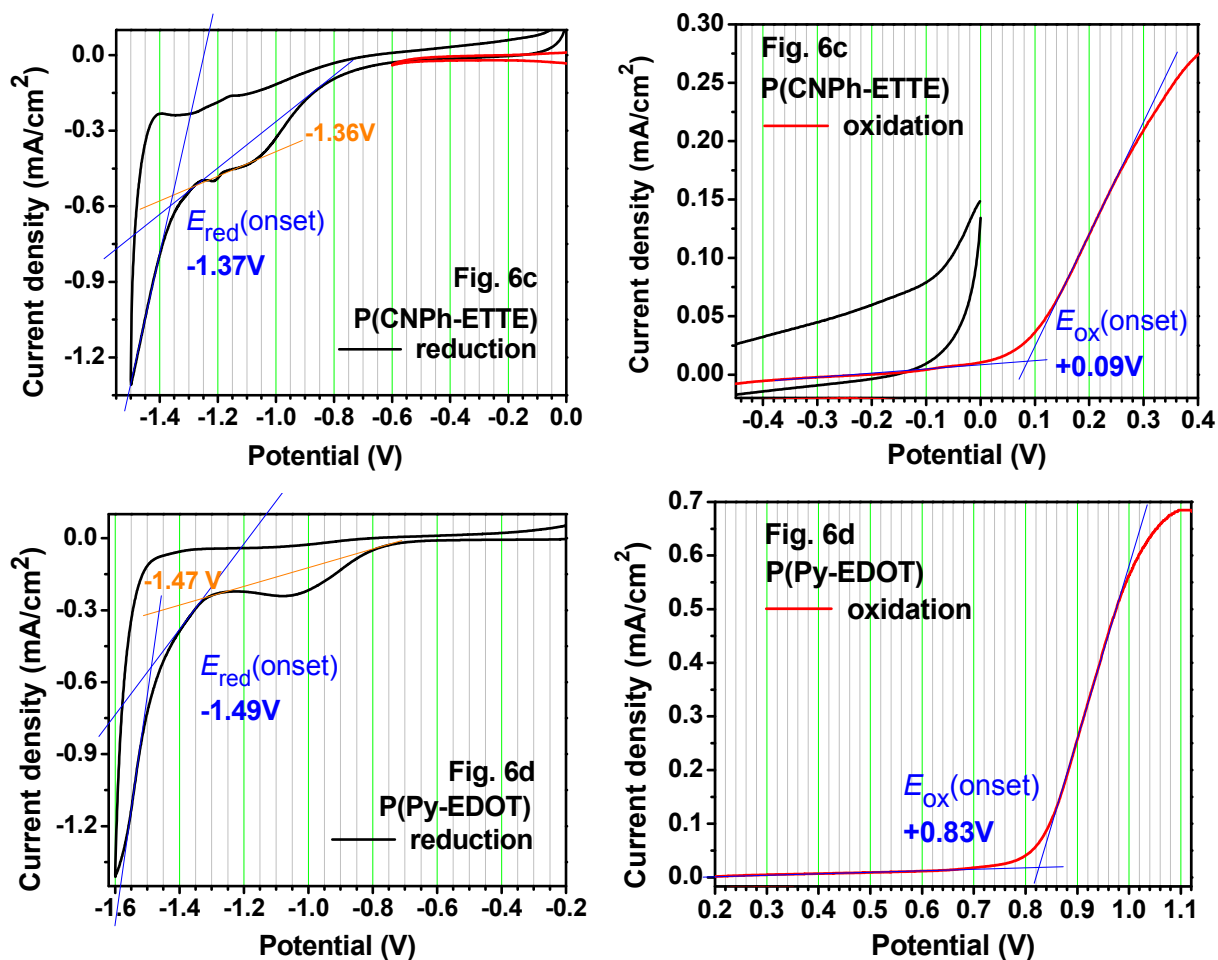


Fig. S20 Expansions of the oxidation and reduction regions for **P(CNPh-ETTE)** and **P(Py-ETTE)** presented in Fig. 6c,d and estimations of their redox potential onsets.

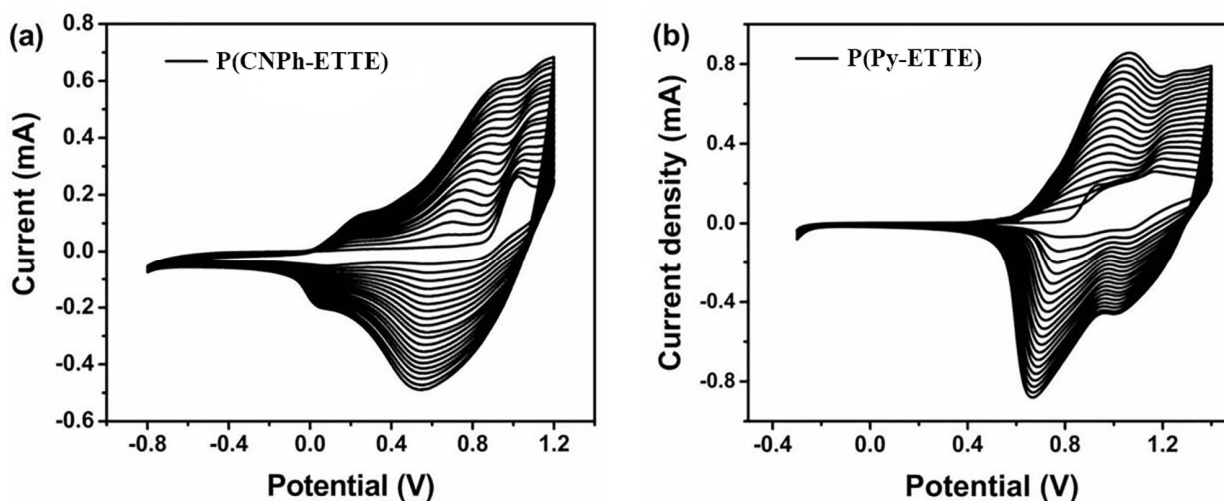


Fig. S21 Electrochemical polymerization of 0.6 mM monomers (a) **CNPh-ETTE** (solvent: CHCl_3/ACN , 75/25, v/v) and (b) **Py-ETTE** (solvent: DCM/THF , 60/40, v/v) with TBAPF_6 (0.1 M) on ITO-coated glass slide at 100 mV/s.

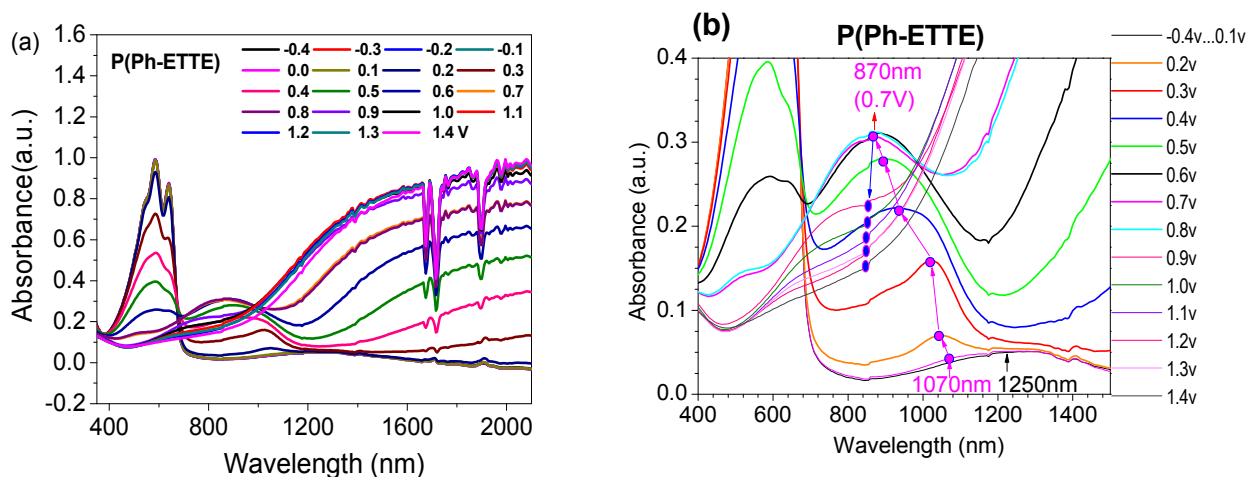


Fig. S22 (a) Spectroelectrochemistry of **P(Ph-ETTE)** film electrochemically deposited on ITO-coated glass slides in a monomer-free ACN/TBAPF₆ (0.1 M) solution, from -0.4 to $+1.4$ V; (b) an expansion of the polaronic absorption region showing the growth and disappearance of the polaronic band during an oxidation.

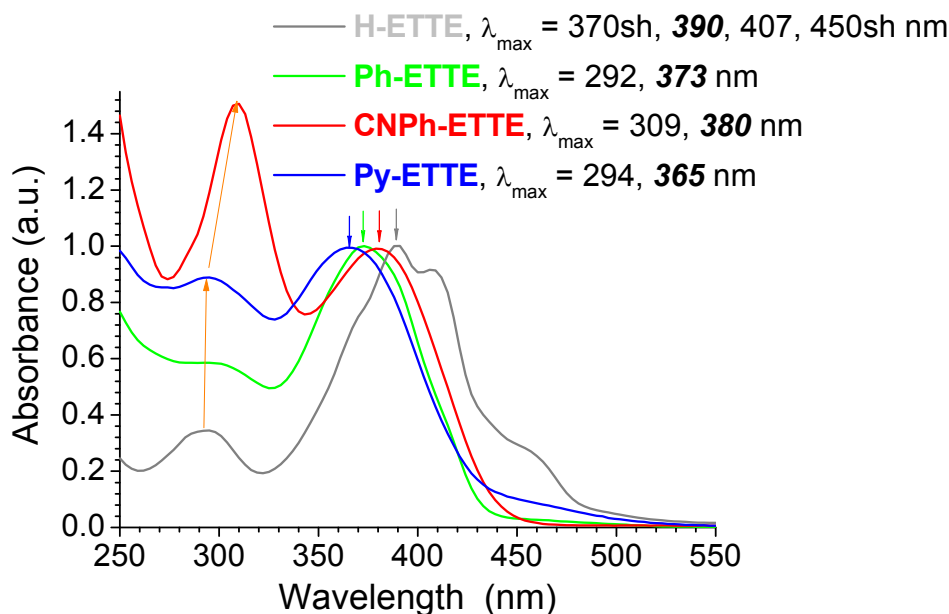


Fig. S23 UV-Vis absorption spectra of monomers in CHCl₃ (spectra are normalized to the longest wavelength absorption maxima): 3,6-substitution in **H-ETTE** monomer with aryl groups (Ph, CNPh, Py) leads to: (i) disappearance of the vibronic structure of the longest absorption π - π^* band, (ii) hypsochromic shift of the longest absorption maxima, (iii) an increase of the intensity of the short wavelength absorption band versus the long wavelength absorption band.

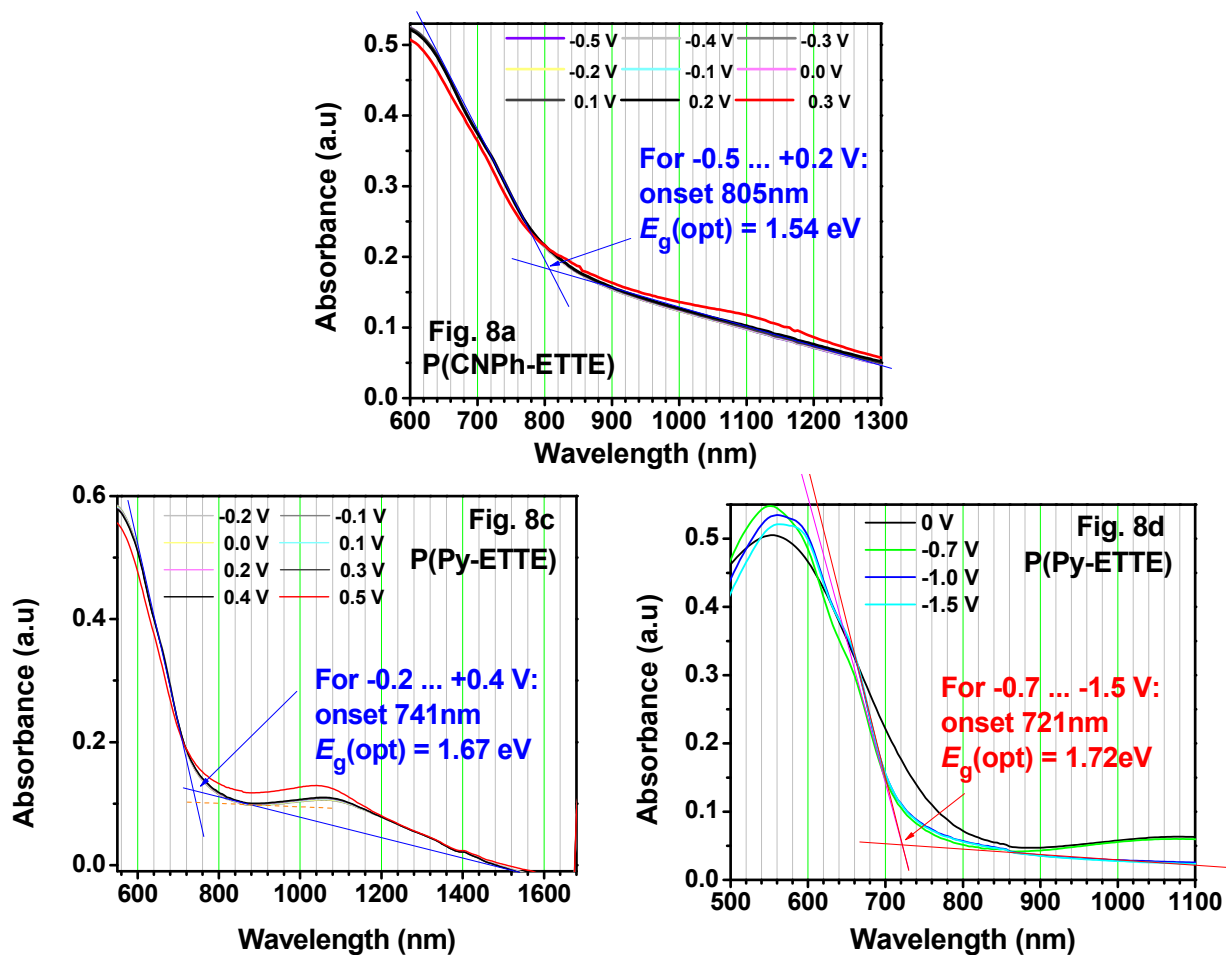


Fig. S24 Expansions of the absorption spectra from SEC experiments presented in Fig. 8a,b,d and estimations of the optical energy gaps for P(CNPh-ETTE) and P(Py-ETTE).

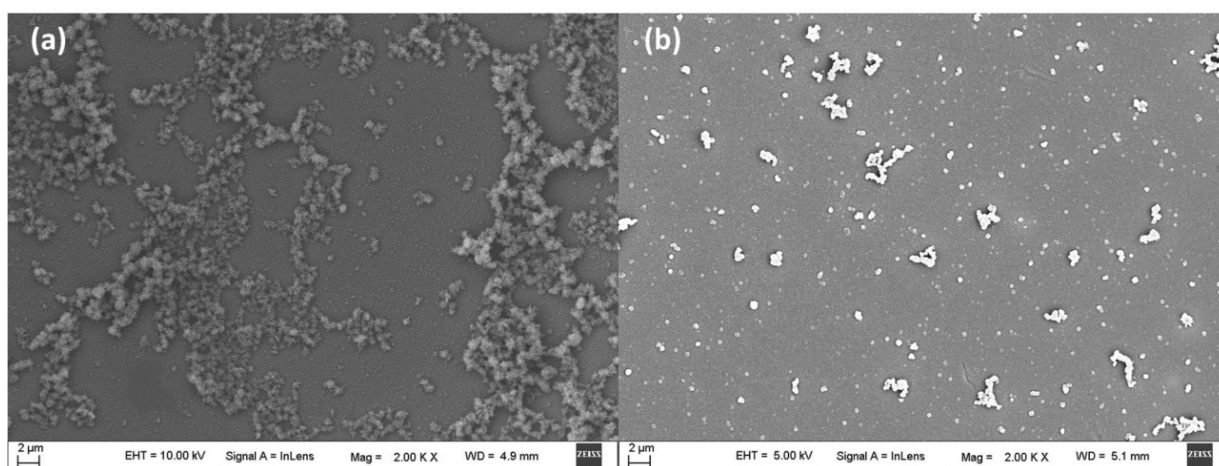


Fig. S25 SEM topography images (magnification 2000 \times) of polymer-coated ITO films: (a) P(CNPh-ETTE), (b) P(Py-ETTE).

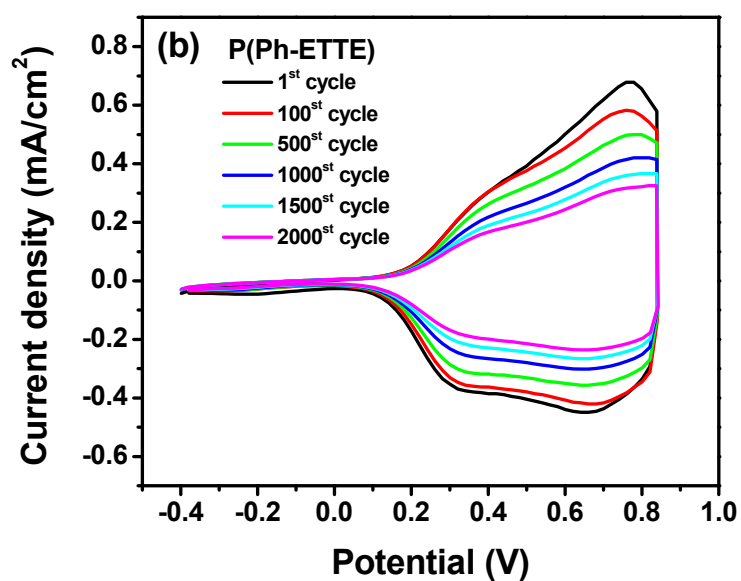
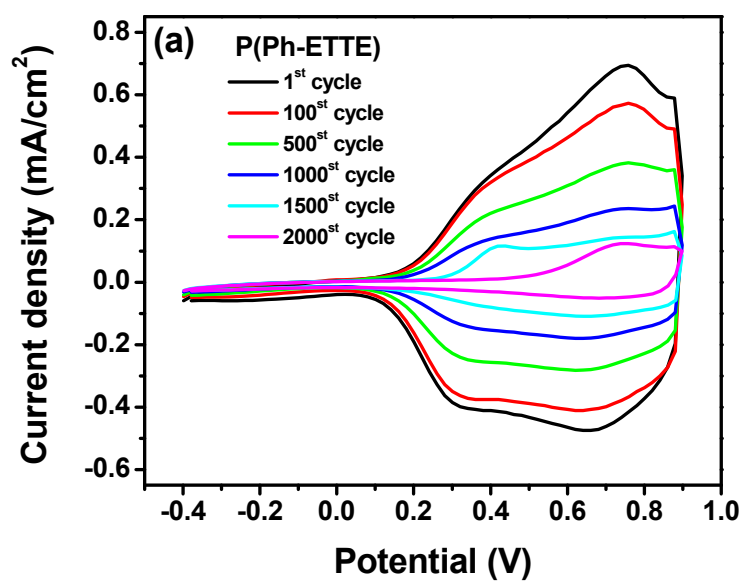


Fig. S26 Stability tests for the **P(Ph-ETTE)** polymer films on the Pt electrode using CV method in a monomer-free ACN/TBAPF₆ (0.1 M) solution at 150 mV/s under ambient condition: (a) cycled 2000 times between -0.4 and 0.9 V; (b) cycled 2000 times between -0.4 and 0.85 V.